Evolution of metamorphic fluid recorded in granulite facies metacarbonate rocks from the middle segment of the Mogok metamorphic belt in central Myanmar

Ye Kyaw Thu[1,*] AND M. ENAMI[2]

[1] Department of Earth and Planetary Sciences, Graduate School of Environmental Studies, Nagoya University, Nagoya 464-8601, Japan

[2] Institute for Space–Earth Environmental Research, Nagoya University, Nagoya 464-8601, Japan (enami@nagoya-u. jp)

* *Present Address*: Department of Geology, Magway University, Taungdwin Road, Magway Region, Myanmar

Short title: FLUID COMPOSITIONS OF MOGOK GRANULITES

ABSTRACT

The Mogok metamorphic belt of Paleogene age, which records subduction- and collision-related events between the Indian and Eurasian plates, lies along the western margin of the Shan plateau in central Myanmar and continues northwards to the eastern Himalayan syntaxis. Reaction textures of clinohumite- and scapolite-bearing assemblages in Mogok granulite facies metacarbonate rocks provide insights into the drastic change in fluid composition during exhumation of the collision zone. Characteristic high-grade assemblages of marble and calc-silicate rock are clinohumite + forsterite + spinel + phlogopite + pargasite/edenite + calcite + dolomite and scapolite + diopside + anorthite + quartz + calcite, respectively. Calculated petrogenetic grids in CaO-MgO-Al_2O_3-SiO_2-H_2O-CO_2 and subsets of this system were employed to deduce the pressure-temperature-fluid evolution of the clinohumite- and scapolite-bearing assemblages. These assemblages suggest higher temperature (> 780–810 °C) and X_{CO2} [= $CO_2/(CO_2 + H_2O)$ > 0.17–0.60] values in the metamorphic fluid for the peak granulite facies stage, assuming a pressure of 0.8 GPa. Calcite grains commonly show exsolution textures with dolomite particles, and their reintegrated compositions yield temperatures of 720–880 °C. Retrograde reactions are mainly characterized by a reaction zone consisting of a dolomite layer and a symplectitic aggregate of tremolite and dolomite grown between clinohumite and calcite in marble, and a replacement texture of scapolite by clinozoisite in calc-silicate rock. These textures indicate that the retrograde reactions developed under lower temperature (< 620 °C) and X_{CO2} (< 0.08–0.16) conditions, assuming a pressure of 0.5 GPa.

The metacarbonate rocks share metamorphic temperatures similar to the Mogok paragneiss at the peak granulite facies stage. The X_{CO2} values of the metacarbonate rock

at peak metamorphic stage are, however, distinctly higher than those previously deduced from carbonate mineral-free paragneiss. Primary clinohumite, phlogopite, and pargasite/edenite in marble have F-rich compositions, and scapolite in calc-silicate rock contains Cl, suggesting a contrast in the halogen compositions of the metamorphic fluids between these two lithologies. The metamorphic fluid compositions were probably buffered within each lithology, and the effective migration of metamorphic fluid, which would have extensively changed the fluid compositions, did not occur during the prograde granulite facies stage throughout the Mogok metamorphic belt. The lower X_{CO2} conditions of the Mogok metacarbonate rocks during the retrograde stage distinctly contrast with higher X_{CO2} conditions recorded in metacarbonate rocks from other metamorphic belts of granulite facies. The characteristic low X_{CO2} conditions were probably due to far-ranging infiltration of H_2O-dominant fluid throughout the middle segment of the Mogok metamorphic belt under low-amphibolite facies conditions during the exhumation and hydration stage.

KEYWORDS: clinohumite; scapolite; granulite facies; metamorphic fluid; Mogok metamorphic belt

1 | INTRODUCTION

Metamorphic fluid effectively transports heat and elements during metamorphism, and its chemical composition is one of the most important factors controlling the stability of mineral assemblages (e.g., Carmichael, 1970; Connolly & Trommsdorff, 1991; Ferry, 1994; Valley, 1986). In particular, metamorphosed carbonate rock typically yields various compositions of CO_2-bearing fluid by decarbonation and dehydration processes, and infiltration of these fluid phases have significant effects on the mineral parageneses of the surrounding lithologies by fluid–rock interaction. Studies of metacarbonate rocks have proved useful in determining the pressure (*P*)–temperature (*T*)–fluid history of high-grade metamorphic regions (Buick, Cartwright & Williams, 1997; Dasgupta, 1993; Faryad, 2002; Gallien, Mogessie, Bjerg, Delpino & de Machuca, 2009; Harley, Fitzsimons & Buick, 1994; Motoyoshi, Thost & Hensen, 1991; Piazolo & Markl, 1999; Satish-Kumar, Wada, Santish & Yoshida, 2001; Warren, Hensen & Ryburn, 1987). In the case of granulite facies metamorphism, F- and Cl-substitutions of OH effectively enlarge the stability fields of hydrous silicates, such as amphibole and biotite, towards high temperature (e.g., Bose, Das & Fukuoka, 2005; Higashino, 2013; Motoyoshi & Hensen, 2001; Pan & Fleet, 1996; Tsunogae *et al*., 2003).

Clinohumite is a typical mineral in metacarbonate rocks of granulite facies, and its F concentration strongly controls the stabilities of clinohumite itself and, eventually, of the mineral parageneses in silica-undersaturated systems (Rice, 1980). Scapolite, which contains Cl and CO_3 as major components, is a main constituent phase of some calc-silicate rocks, and its occurrence provides a strong constraint on metamorphic temperature and fluid composition (e.g., Harley *et al*., 1994; Moecher & Essene, 1990; Satish-Kumar & Harley, 1998). Evolution of metamorphic fluid compositions has been

discussed for metacarbonate rocks from many granulite facies regions: e.g., India (Satish-Kumar, Santosh, Harley & Yoshida, 1996; Satish-Kumar *et al*., 2001), Africa (Kaneko, Miyano & Tsunogae, 2005), Antarctica (Satish-Kumar, Hermann, Tsunogae & Osanai, 2006), and Australia (Buick *et al*., 1997). Most of these studies have considered recrystallizations under extremely high X_{CO2} [= $CO_2/(CO_2 + H_2O)$] fluid conditions at the granulite facies stage as well as the subsequent retrograde stage. However, Buick, Cartwright and William (1997) reported that metacarbonates of the Reynolds Range group (~0.5 GPa/750–800 °C) that initially equilibrated at $X_{CO2} > 0.8$ were mineralogically reset by local infiltration of H_2O-rich fluids ($X_{CO2} \leq 0.02$–0.3) at 0.3–0.4 GPa/650–700 °C along narrow strike-parallel zones.

Granulite facies metamorphic rocks occur extensively in the middle segment of the Late Eocene–Late Oligocene Mogok metamorphic belt in Myanmar, which formed during subduction and collision between the Indian and Eurasian plates. Metacarbonate rocks containing F-rich clinohumite or scapolite commonly occur in the granulite facies area. These samples also preserve reaction textures of retrograde stages and provide information for understanding the evolution of *P*-*T*-fluid conditions during exhumation. The present study reports the compositional characteristics and modes of occurrence of clinohumite, scapolite, and associated minerals in the metacarbonate rocks and discusses changes of metamorphic fluid compositions from high-X_{CO2} at the peak metamorphic stage to low-X_{CO2} during exhumation and a retrograde low-amphibolite facies stage. These facts mean that firstly, the metamorphic fluid compositions were internally buffered within each lithological unit and the effective migration of metamorphic fluid did not occur during the peak granulite facies stage, and secondly, their high X_{CO2} composition were extensively reset to low X_{CO2} during the retrograde

stage by infiltration of H_2O-rich fluid phases beyond the lithologic boundaries throughout the Mogok metamorphic belt. Abbreviations for the minerals and endmembers described in the text, figures, and tables are after Whitney and Evans (2010).

2 | GEOLOGICAL SETTING

2.1 | Mogok metamorphic belt

Myanmar is geologically divided into Eastern and Western provinces, separated by the 1200 km long, N-S trending Sagaing dextral strike-slip fault (Figure 1). The Western province, or Burma microplate, includes the Indo-Burma Ranges and Central Myanmar basins. The Indo-Burma Ranges, where the Burma microplate overrides the Indian oceanic crust, consist of Late Cretaceous to Paleogene marine sediments and stratigraphically lower flysch-type sediments (Acharyya, 2007; Gardiner, Searle, Robb & Morley, 2015; Ghose, Chatterjee & Fareeduddin, 2013). The Central Myanmar Basin is covered by a series of Cretaceous to Pleistocene sediments and Quaternary volcanic rocks (Mitchell, 1993). The Eastern province is a part of the Shan-Thai block that collided with the Indochina block in the Early or Late Triassic (Metcalfe, 1988, 2000; Mitchell, 1977). It comprises the Shan plateau, the Slate belt (or Mergui Group), and the Mogok metamorphic belt (Figure 1). Most of the Shan plateau is characterized by an Upper Cambrian to Lower Cretaceous succession (Boucot, 2002), overlying metamorphic rocks of the Chaung Magyi Group. The Slate belt also consists of distinctive Late Paleozoic glacial marine pebbly mudstones that extend to Thailand, the Malay Peninsula, and Sumatra (Barber & Crow, 2009; Ridd & Watkinson, 2013).

The Mogok metamorphic belt extends along the northwestern margin of the Shan plateau and west of the Slate belt, reaching 1500 km in length (Mitchell *et al*., 2007; Searle *et al*., 2007). This belt consists of a series of undifferentiated high-grade metasedimentary and meta-igneous rocks, and common lithologies include a variety of gneiss, schist, quartzite, marble, calc-silicate rock, and migmatite with various granitoid intrusions (Barley, Pickard, Khin Zaw, Rak & Doyle, 2003; Mitchell *et al*., 2007; Searle *et al*., 2007). Radiometric dating focused on the metamorphic and tectonic evolution of the Mogok belt and adjacent areas has been discussed by many researchers. Bertrand *et al*. (1999) and Bertrand, Rangin, Maluski and Bellon (2001) reported Oligocene to Middle Miocene ages based on Ar-Ar and K-Ar analyses of biotite and muscovite, and proposed the northward passage of the eastern Himalayan syntaxis, characterized by crustal thinning, resulting from the India–Asia oblique collision. Sensitive high-resolution ion microprobe (SHRIMP) U-Pb dating of zircon obtained from granites indicates that the magmatism occurred during the Jurassic and a later high-grade metamorphic recrystallization event took place during the Eocene (Barley *et al*., 2003). Garnier, Maluski, Giuliani, Ohnenstetter and Schwarz (2006) reported Ar-Ar ages of 18.7 – 17.1 Ma on phlogopite in ruby-bearing marble near Mogok. Searle *et al*. (2007) reported U-Th-Pb ages of metamorphic monazite, zircon, xenotime, and thorite employing isotope dilution thermal ionization mass spectrometry (ID-TIMS) and laser ablation–multicollector–inductively coupled plasma mass spectrometry (LA-MC-ICPMS), and suggested two distinct metamorphic events: firstly, a Paleocene event, which implies earlier regional metamorphism (~59 Ma); and secondly, a Late Eocene to Oligocene event, which was interpreted as the peak metamorphic stage resulting in synmetamorphic crustal melting which produced garnet- and

tourmaline-bearing leucogranite (~24.5 Ma). Maw Maw Win, Enami and Kato (2016) also dated the metamorphic monazite using U-Th-Total Pb Chemical Isochron Method (CHIME: Montel *et al*., 2017 in press; Suzuki & Adachi, 1991) and reported the peak metamorphic stage for upper-amphibolite and/or granulite facies as Late Eocene and the subsequent hydration stage as Late Oligocene. The youngest magmatic event indicated was Late Oligocene–Early Miocene, producing mantle-derived syntectonic hornblende syenite and crust-derived leucogranite, postdating the high temperature metamorphism and intrusion (Barley *et al*., 2003; Bertrand *et al*., 1999; Searle *et al*., 2007). These ages suggest that the belt has experienced a complex series of tectonic, magmatic and metamorphic events with subsequent post collisional extension, up-lift, and exhumation processes.

2.2 | Onzon–Thabeikkyin region

The Onzon, Wabyudaung, Zayetkwin, Aung Tharyar, and Thabeikkyin areas, from which the samples were collected, are located about 100 km north of the Mandalay region and belong to the middle segment of the Mogok metamorphic belt (Figure 2a). These areas are denoted as the Onzon–Thabeikkyin region, hereafter, unless otherwise noted. Paragneiss, marble, and calc-silicate rock occupy the middle segment of the Mogok metamorphic belt from Mandalay to Mogok regions (Maw Maw Win *et al*., 2016; Maw Maw Win, Enami, Kato & Ye Kyaw Thu, 2017; Ye Kyaw Thu, Enami, Kato & Tsuboi, 2017; Ye Kyaw Thu, Maw Maw Win, Enami & Tsuboi, 2016; Yonemura *et al*., 2013), continuing southward, where they become less dominant. The metamorphic lithologies in this region form a zone with an average width of 40 km and consist of various types of marble and calc-silicate rock with paragneiss of granulite

facies. The typical mineral assemblage of the paragneiss is Grt-Bt-Pl-Sil-Qz; cordierite and spinel are included in some samples. Biotite grains coexisting with rutile and/or ilmenite have a high TiO_2 content, of up to 6.9 wt% (Ye Kyaw Thu *et al*., 2016). Conventional geothermobarometers and Zr-in-rutile geothermometers yield *P-T* conditions of 0.60–0.84 GPa/780–860 °C as the peak granulite facies metamorphism (Ye Kyaw Thu *et al*., 2016, 2017). These paragneiss were extensively recrystallized under lower-amphibolite facies conditions (about 0.40–0.55 GPa/620–640 °C) during the exhumation and hydration stage.

In the Onzon–Thabeikkyin region, the metacarbonate rocks occur in a zone of 10–15 km width, which is wedged between paragneiss (Figure 2b). Myint Lwin Thein, Ohm Myint, Sun Kyi and Hpone Myint Win (1990) divided these metamorphic rocks into the Wabyudaung and Thabeikkyin Subgroups, which consist of Kantha, Tesoegyi, Sakantha, and Kyetsaung Taung marble units and paragneiss and calc-silicate and diopside marble units, respectively. The metacarbonate rocks widely occur as massive or thick-layered forms and are locally intruded by granitoid rocks. The plutonic rocks are grouped into biotite microgranite (Kabaing granite), leucogranite, syenite, and pegmatite. The syenitic rocks occasionally include xenoliths of marble and calc-silicate rock, and their U-Pb zircon ages yield ~30.9 Ma (Barley *et al*., 2003). The Kabaing granite, which is a major plutonic lithology, intrudes into metamorphic rock units and parts of the syenite and leucogranite, and shows no sign of tectonic deformation. U-Pb zircon and Ar-Ar biotite ages of the Kabaing granite are 16.8 ± 0.3 Ma (Gardiner *et al*., 2016) and 15.8 ± 1.1 Ma (Bertrand *et al*., 2001), respectively. Later-stage pegmatitic rocks locally intrude into the Kabaing granite as dykes or veins, and grade into quartz vein or syenite pegmatite.

Samples studied were collected from the Kyetsaung Taung marble unit of the Wabyudaung Subgroup and the calc-silicate and diopside marble units and paragneiss unit of the Thabeikkyin Subgroup (Figure 2b). The Kyetsaung Taung marble unit is composed of major coarse-grained white marble consisting mostly of monomineralic calcite grains and a small amount of impure marble containing calcite, diopside, phlogopite, forsterite, humite, spinel, and graphite. This marble is massive and is exposed as discontinuous bands trending ENE–WSW. Fine-grained marble and graphite-marble are locally intercalated within this marble unit. The calc-silicate rock unit forms a mappable zone, which can be traced continuously throughout the sampling area, and is usually associated with a small amount of diopside marble, phlogopite marble, and graphite marble. Thin quartzo-feldspathic bands with mica are locally interbedded with the impure marble. Skarn is developed in the calc-silicate rock around the Kabaing granite intrusion. Lenticular clots of graphite occur in metacarbonate rocks adjacent to the boundary with the paragneiss unit. The paragneiss unit in the Thabeikkyin area is mainly composed of highly weathered garnet-biotite paragneiss with occasional intercalations of biotite paragneiss and leucogneiss.

3 | PETROGRAPHY OF METACARBONATE ROCKS

Four samples of dolomite-bearing marble (KST03, ZYK01, OZ01, and ACT01) and three samples of calc-silicate rock (OZ03, WBY01, and KB01) were selected for detailed analyses (Figure 2b). The mineral assemblages of the marble and calc-silicate rock samples are listed in Table 1.

3.1 | Forsterite-bearing marble

The forsterite-bearing marble samples, KST03 (96°04'35" E, 22°50'22" N) and ZYK01 (96°03'54" E, 22°49'06" N), were collected from the Kyetsaung Taung marble unit in the Zayetkwin area (Figure 2b). They are medium- to coarse-grained with granoblastic and polygonal texture, and are characterized by the assemblage of Cal + Dol + Chu + Fo + Spl + Amp + Phl + Gr (Figure 3) and Cal + Dol + Fo + Spl + Phl, respectively (Figure 4a and b). Calcite is coarse-grained (0.2–1 mm in size) and usually occurs as a matrix phase (Figures 3a–c and e, and 4a and b) and as inclusions in clinohumite (Figure 3a), spinel (Figures 3d and 4a), and forsterite (Figure 4b). In KST03, calcite also occurs as a retrograde product replacing dolomite (Figure 3c). The calcite grains included by clinohumite and other phases exhibit exsolution particles of dolomite. The matrix calcite grains in ZYK01 show a dolomite exsolution texture (Figure 4a and b) as do calcite inclusions. However, in KST03, the matrix (Figure 3a, c) and retrograde (Figure 3c) calcite grains, do not show such an exsolution texture, except for a narrow marginal zone (100–200 μm in width) around some matrix grains (Figure 3e). Dolomite grains usually occur as exsolution products in calcite (Figures 3d and 4a, d) and isolated grains in the matrix (Figures 3c and 4a–c), which might be partly the result of coalescence of exsolved dolomite. In KST03, dolomite grains additionally occur as reaction products between calcite and clinohumite (Figure 3a and b). The dolomite grains of reaction products are texturally divided into those that occur as isolated zones (Figure 3a and b) and as symplectitic aggregates with tremolite (Figure 3a, b, and f). The dolomite-tremolite symplectites rarely contain diopside (Figure 3a and e), in which diopside is always surrounded by tremolite (Figure 3e).

Spinel grains occur as prismatic porphyroblasts (Figures 3c and 4a: up to 3 mm in diameter) and inclusions (200 μm in width) in clinohumite (Figure 3b). In ZYK01,

forsterite grains occur as stable phases and tend to form irregular- or granular-shaped grains (0.3–3 mm in diameter) (Figure 4b), and partly pseudomorphed or altered to serpentine (Figure 4a and b). In contrast, only small granular-shaped forsterite inclusions (50–500 μm) were observed in the clinohumite porphyroblasts in KST03 sample (Figure 3a and b). Granular- or irregular-shaped clinohumite grains (2–3 mm in size) occur as a major phase in KST03 and are always rimmed by a zone which consists of dolomites and symplectitic aggregates of tremolite and dolomite (Figure 3a, b, and f). This intergrowth zone borders clinohumite with calcite, texturally indicating a reaction product of clinohumite and calcite. Most clinohumite grains include small and granular forsterite grains indicating that these two phases were in equilibrium during the prograde stage (Figure 3a and b). Although tremolite commonly forms symplectite with dolomite around clinohumite crystals (Figure 3f), primary pargasite/edenite is also observed around spinel grains in association with phlogopite and chlorite in KST03 (Figure 3c). Phlogopite also occurs as a matrix phase in ZYK01 (Figure 4a). Chlorite flakes occur between spinel and clinohumite/dolomite grains (Figure 3b) and as rim phase around pargasite/edenite (Figure 3c).

3.2 | Forsterite-free marble

The forsterite-free marble samples (OZ01 and ACT01) were collected from calc-silicate and diopside marble unit in the Onzon (96°05'32" E, 22°48'50" N) and Aung Tharyar (96°00'19" E, 22°53'08" N) areas, respectively (Figure 2b). The main mineral assemblages of these samples, OZ01 and ACT01, are Cal + Dol + Spl + Phl (Figure 4c) and Cal + Di + Phl + Prg (Figure 4e), respectively. In OZ01, calcite grains, which exhibit an exsolution texture with dolomite, are the major matrix phase and also occur

as inclusions in spinel (Figure 4c and d). Although relatively coarse dolomite grains (up to 700–800 μm) were observed in the matrix of OZ01, they were always surrounded by calcite or occurred as an interstitial phase between calcite and silicate phases (Figure 4c and d). Therefore, the coarse-grained dolomite in the matrix might have been the result of coalescence of exsolved dolomite; there are no isolated primary dolomite grains in OZ01. Calcite grains of both inclusion and matrix phases in ACT01 do not exhibit a significant dolomite exsolution texture, although some parts of the matrix grains contain small amounts of exsolved dolomite (Figure 4f).

Prismatic spinel grains (up to 0.6 mm in size) are observed in OZ01 and commonly include calcite grains with dolomite exsolution particles (Figure 4c). Large flakes of phlogopite are dominant in the matrix in both samples (Figure 4c and e), and also observed as aggregates associated with spinel in OZ01 and with diopside in ACT01. Diopside grains occur as granular- or anhedral-shaped grains of 0.3–1 mm in size in ACT01. They commonly form aggregates with calcite, phlogopite, and pargasite, and some grains include isolated calcite grains (Figure 4e). In ACT01, secondary tremolite partially replaces diopside around the margins. Chlorite occurs as a secondary phase replacing some fine-grained spinel grains in OZ01.

3.3 | Calc-silicate rock

Calc-silicate rock samples were collected from the calc-silicate and diopside marble unit in the Onzon (OZ03: 96°05'37" E, 22°48'48" N) and Wabyudaung (WBY01: 96°06'34" E, 22°52'07" N) areas, and the paragneiss unit in the Thabeikkyin (95°58'59" E, 22°53'18" N) area (Figure 2b). They are fine to medium-grained and show granoblastic textures. The main mineral assemblage of these samples is Scp + Di

+ Cal + Qz + Kfs + Ttn (Figure 5a). Scapolite is a major primary phase in all calc-silicate rock samples and occurs as subhedral to anhedral grains of 0.1– 0.7 mm in size. Some scapolite grains in OZ03 show optical zoning consisting of a primary core and a thin meionite rim (Figure 5a). The primary scapolite grains in WBY01and KB01 were retrogressively replaced by plagioclase with minor amounts of calcite and quartz (Figure 5b) and clinozoisite (Figure 5c), respectively. Coarse plagioclase grains, which are partly replaced by aggregates of muscovite and quartz, occur as inclusions in calcite of WBY01 (Figure 5d). An aggregate of plagioclase with scapolite and/or K-feldspar was also included in the calcites of WBY01, and no distinct reaction relationship was observed between them (Figure 5b). These textural characteristics suggest that these plagioclase grains were primary phase and in equilibrium with scapolite. The matrix diopside grains are rounded granular matrix minerals and range from 0.4 – 1.7 mm in size. Those in OZ03 show subhedral porphyroblasts and enclose scapolite, calcite, quartz, and titanite. Although most of the diopside grains in OZ03 are partly replaced by tremolite, those in WBY01 and KB01 show no replacement or pseudomorph texture. In OZ03 and WBY01, quartz is the dominant phase and coexists with scapolite, diopside and calcite (Figure 5a), whereas the quartz modal composition of KB01 is less than 1 vol%. Clinozoisite occurs only in KB01, which is texturally differentiated into two domains: one is dominated by scapolite, diopside, titanite, and small amounts of quartz and calcite and the other is characterized by almost monomineralic clinozoisite (> 3 mm in diameter) with scapolite and calcite relics (Figure 5c). Titanite grains occur as rounded and subhedral crystals in the matrix of all of the studied samples (Figure 5a). They also occur as inclusions in the scapolite and diopside/clinozoisite of OZ03 and KB01, respectively.

4 | MINERAL CHEMISTRY

The constituent minerals in the marble and calc-silicate rock were analyzed using the JEOL JXA-8800R (WDS + EDS) electron-probe microanalyzer (EPMA) at the Department of Earth and Planetary Sciences of Nagoya University. The accelerating voltage and specimen current for the quantitative analyses were maintained at 15 kV and 12 nA on the Faraday cup, respectively. Beam diameters of 10 and 5 μm were used for calcite and mica/feldspar analysis, respectively, and diameters of 2–3 μm were used for the analyses of all other phases. Well-characterized natural and synthetic phases, including synthetic F-phlogopite (F = 8.7 wt%) for F and natural Cl-rich hastingsite (Cl = 3.27 wt%: Suwa, Enami & Horiuchi, 1987) for Cl, were employed as standards. Matrix corrections were performed using the α-factor table of Kato (2005). The representative chemical analyses of the major constituent minerals of the marble and calc-silicate rock samples are listed in Tables 2 and 3, respectively. The Fe^{3+}/Fe^{2+} value for amphibole was estimated considering an average of the minimum and maximum values proposed by Leake *et al*. (1997) and that for spinel was estimated assuming stoichiometry and a charge balance. The total iron content was assumed to be in the form of Fe_2O_3 for clinozoisite and titanite and FeO for the other phases.

4.1 | Clinohumite

Clinohumite grains from the Mogok marble are compositionally homogeneous and have an M_{Ti}/Si value of 2.22 ± 0.02 (Figure 6), where M_{Ti} denotes the total octahedral cations including Ti (Gaspar, 1992; Jones, Ribbe & Gibbs, 1969). This compositional range is consistent with those of titanian clinohumite from the carbonatites of the Jacupiranga

Complex of Brazil (2.22 ± 0.03: Gaspar, 1992) and F-rich clinohumite from the Ambasamudram marble of Southern India (2.22 ± 0.01 for low M_{Ti}/Si group data: Satish-Kumar & Niimi, 1998). The humite group minerals consist of laminations of olivine and brucite layers, and their compositions are characterized by the number "*n*", which indicates the ratio of these two layers [$n(M, Fe)_2SiO_4 \bullet (Mg, Fe)(F, OH)_2$] (Jones *et al*., 1969). From their stoichiometry, the relationship of M_{Ti}/Si with n is

$$\frac{M_{Ti}}{Si} = \frac{(2n+1)}{n}$$

Most of the M_{Ti}/Si values from the Mogok samples fall below the expected value of 2.25 ($n = 4$) that would be the minimum for the humite group minerals, indicating the presence of superstructures with $n > 4$ in the analyzed clinohumite (e.g., Gaspar, 1992). The spots with lower M_{Ti}/Si values correspond to clinohumite phases where the stacking sequence is mainly made up of $n = 4$ and 6 in different proportions for each superstructure (e.g., White & Hyde, 1982). The TiO_2 and FeO contents are less than 0.15 wt% and 0.36 wt%, respectively, and X_{Mg} [= Mg/(Mg + Fe)] = 1.00. The F and Cl contents are 3.57–4.14 wt% [X_F = F/2 for O = 17 ≈ F/(F + Cl + OH) = 0.62 ± 0.03] and less than 0.02 wt%, respectively.

4.2 | Phlogopite

Phlogopite grains have near Mg-endmember compositions (X_{Mg} = 0.96–1.00) and are rich in F (1.4–3.6 wt%). The average X_F values for KST03, ZYK01, OZ01, and ACT01 are 0.77 ± 0.06, 0.38 ± 0.03, 0.44 ± 0.04, and 0.50 ± 0.03, respectively (Figure 7a). Chlorine contents are typically less than 0.05 wt% in all samples. The average TiO_2 content varies from 0.16 ± 0.02 wt% in ZYK01 to 0.81 ± 0.05 wt% in OZ01. Although

the CaO content is less than 0.1 wt% in all samples, BaO and Na_2O contents reach 7.9 wt% [0.22 atomic per formula unit (apfu) for O = 11] and 1.36 wt% (0.19 apfu) in KST03 (Figure 7b). The phlogopite grains in ZYK01 also contain up to 1.1 wt% (0.16 apfu) Na_2O. Barium incorporation into Ti-poor phlogopite is generally controlled by the following substitutions: $Ba\square K_{-2}$ and $BaAlK_{-}Si_{-1}$, where □ indicates a vacant site (e.g., Fleet, 2003). The (Ba + Ca)–(K + Na) diagram suggests that Ba-substitution of phlogopite in KST03 is promoted by the combination of these two types of substitutions (Figure 7c). (Ba + Ca) > (3-Si) compositions (for O = 11) in some Ba-rich grains (Figure 7d) are consistent with this interpretation. However, the compositional trend of some Ba-rich grains with (Ba + Ca) < (3-Si) cannot be explained by these Ba-bearing substitutions alone. Considering the compositional trend subparallel to the Si-axis, the compositional varieties of the Ba-rich phlogopite of KST03 were mainly controlled by combinations of three types of substitutions, including the tschermakite substitution ($Al_2Mg_{-1}Si_{-1}$).

4.3 | Forsterite and spinel

Forsterite grains have endmember compositions of X_{Mg} = 0.99–1.00, and their NiO, MnO, and CaO contents are below the detection limit of about 0.03 (CaO)–0.04 (NiO and MnO) wt% (2σ level).

Spinel grains also have near endmember compositions of X_{Mg} = 0.90–1.00 and X_{Al} [= Al/(Al + Fe^{3+} + Cr + V)] = 0.98–1.00. The V_2O_3 content reaches 1.3 wt% in KST03, and the ZnO content is up to 2.2 wt% in OZ01. These components, however, are usually less than 0.1 wt% and 0.5 wt% in other samples, respectively.

4.4 | Scapolite, plagioclase, and K-feldspar

Primary scapolite grains are relatively homogeneous and exhibit a solid solution mainly between meionite ($Ca_4Al_6Si_6O_{24}CO_3$) and mizzonite ($NaCa_3Al_5Si_7O_{24}CO_3$), with equivalent anorthite (*EqAn*) = 65–72 and X_{Cl} = 0.05–0.07 in OZ03; *EqAn* = 73–77 and X_{Cl} = 0.01–0.02 in WBY01; and *EqAn* = 69–73 and X_{Cl} = 0.08–0.11 in KB01, where *EqAn* = (Al-3)/3 × 100 and X_{Cl} = Cl/2 for total cations = 16 ≈ Cl/(Cl + CO_3) (Figure 8). The primary core of scapolite in OZ03 was retrogressively rimmed by a marialite ($Na_4Al_3Si_9O_{24}Cl$)-rich mantle with *EqAn* = 33–51 and X_{Cl} = 0.42–0.78 (Figure 5a). In KB01, scapolite was strongly replaced by clinozoisite (Figure 5c) and has a relatively marialite-richer composition (*EqAn* = 40–65 and X_{Cl} = 0.18–0.51) than the primary phase.

Texturally, primary plagioclase grains (Figure 5b and d) are homogeneous and have mostly near endmember compositions of $An_{90–96}$ (Figure 8). In contrast, plagioclase grains, which retrogressively replaced scapolite (Figure 5b), have a slightly sodic composition with $An_{75–85}$. The orthoclase contents of K-feldspar vary from $Or_{87–93}$ in OZ03 to $Or_{94–96}$ in KB01. The BaO and CaO contents are less than 0.4 wt% and 0.2 wt%, respectively.

4.5 | Amphibole

Amphibole grains in the marble (KST03, ZYK01, and ACT01) are Mg-endmember varieties with X_{Mg} = 0.92–1.00. They are texturally grouped into primary and secondary phases. The primary phases are pargasite/edenite with Si values down to 6.00 apfu (O = 23) and Al and $^{[A]}$(Na + K) values up to 2.90 apfu and 0.97 apfu, respectively, where

$^{[A]}$(Na + K) indicates the alkaline contents at the largest A-site (Figure 9a). In contrast, secondary phases, which replace primary amphibole or are products of the retrogressive reaction of clinohumite and calcite (Figure 3f), are tremolite with Si values mostly greater than 7.48 apfu and Al and $^{[A]}$(Na + K) values less than 0.94 apfu and 0.41 apfu, respectively. The amphibole grains in the marble are characteristically rich in F with X_F = 0.27–0.54 (1.2–2.5 wt%) for the primary phase and 0.11–0.32 (0.51–1.54 wt%) for the secondary phase (Figure 9b). Chlorine contents are less than 0.09 wt% for all grains.

Amphibole grains in the calc-silicate rock (OZ03), which replace diopside, are F-poor tremolite and have slightly lower X_{Mg} values (0.75–0.82) than those in the marble: Si = 7.50–7.87 apfu, Al = 0.20–0.77 apfu, $^{[A]}$(Na + K) = 0.01–0.12 apfu, X_F < 0.02 (< 0.07 wt%), and Cl < 0.02 wt%.

4.6 | Calcite and dolomite

Calcite grains in marble are simple solid solutions between calcite and dolomite with FeO and MnO contents of mostly less than 0.2 wt% (0.3 mol% of siderite) and 0.05 wt% (0.1 mol% of rhodochrosite), respectively. The matrix calcite grains with exsolution textures in ZYK01 and OZ01 are usually divided into core and mantle parts, which are rich and poor in dolomite particles, respectively (Figure 4a, c, and d). The mantle is usually poorer in magnesite content than the core (Figure 4d). Although the exsolved parts of the matrix and inclusion are slightly heterogeneous, the variation of magnesite content is 1–2 mol% in most cases (e.g., Figure 3d). Calcite grains, which contain exsolved dolomite particles, have relatively low magnesite components of less than 5.3–7.5 mol% (Figure 10a–c); whereas some domains, which locally survived the exsolution of dolomite, have higher magnesite contents of 9.4–10.5 mol% (Figure 10b

and c). Isolated calcite grains without dolomite spherules in the matrix of KST03 (Figure 3a, c, and e) have relatively low magnesite contents: up to 7.0 mol%. The matrix calcite grains in ACT01 mostly occur as isolated phases and show little exsolution texture. In the case of locally exsolved calcite in ACT01, the host calcite around the dolomite spherules exhibit locally high calcite content (Figure 4f). However, calcite in points 100–200 μm away from the dolomite has lower calcite composition, and shows continuous variation of up to 9.8 mol% of the magnesite component (Figure 10d). ACT01 contains no primary dolomite in the matrix or the inclusion phase, indicating that the matrix calcite was not saturated in the magnesite component during its formation. The wide compositional ranges and rare development of exsolution textures of the matrix calcite grains in ACT01 might be largely attributed to the undersaturated magnesite environment during the prograde metamorphic stage. The calcite grains included in the diopside of ACT01 do not show exsolution textures and have lower magnesite content (up to 2.7 mol%) than the matrix grains. Texturally retrograde calcite in KST03, which replaces matrix dolomite (Figure 3c), has similar magnesite content (up to 6.4 mol%) to the isolated matrix calcite (Figure 10a).

Calcite grains in the calc-silicate rock have near endmember compositions, and MgO, FeO, and MnO are less than 0.7 wt% (1.5 mol% of magnesite), 1.1 wt% (1.5 mol% of siderite), and 0.2 wt% (0.2 mol% of rhodochrosite), respectively.

Dolomite grains in marble, except those in ACT01, are in simple solid solution, and the FeO and MnO contents are less than 0.3 wt% and 0.05 wt%, respectively. In ACT01, the FeO content reaches 2.5 wt% (3.4 mol% of siderite) and MnO was not detected. Calcite content varies from 52 mol% of ZYK01 to 57 mol% of ACT01 on average, and

does not show distinct differences between exsolved spherules and the isolated phase in the matrix.

Homogeneous calcite compositions prior to the unmixing phenomenon in marble were estimated by reintegration based on: firstly, the average chemical compositions of calcite and dolomite; secondly, their volume ratio estimated using digital back-scattered electron (BSE) images and the image analysis software 'ImageJ 1.51g' (Rasband, W.S., ImageJ, U. S. National Institutes of Health, Bethesda, Maryland, USA, http://imagej.nih.gov/ij/, 1997-2012) (Schneider, Rasband & Eliceiri, 2012); and thirdly, densities of calcite and dolomite of 2.71 and 2.87 g/cm^3, respectively, which were calculated using lattice constants reported by Paquette and Reeder (1990). The estimated volume ratios (V_{Dol}/V_{Cal}) of the inclusion phases are 0.18–0.55, and those of the matrix phases vary from 0.22–0.24 in OZ01 to <0.01 in ACT01.

In KST03, the primary calcite grains included in clinohumite have distinctly more magnesite-rich compositions (20.4 –21.2 mol%) than those in spinel (12.5–13.0 mol%). Conversely, the reintegrated compositions of exsolved calcite grains in the other two samples are relatively constant within each sample and do not show any relationship to their modes of occurrence: ZYK01, 13.3–14.1 mol% for matrix grains, 13.0 and 14.3 mol% for inclusions in spinel, 14.0 and 16.4 mol% for inclusions in forsterite; OZ01, 12.0 and 12.7 mol% for matrix grains and 13.2–14.5 mol% for inclusions in spinel. Although matrix calcite grains in ACT01 locally show exsolution texture, their reintegrated compositions were not estimated because of the very low volume contents of the exsolved dolomite particles ($V_{Dol}/V_{Cal} < 0.01$). However, it is possible that the primary compositions of the calcite grains might have been similar to those of the magnesite-rich part of the isolated grains free of dolomite spherules.

4.7 | Diopside

Primary diopside grains in marble (ACT01) have near endmember composition with X_{Mg} = 0.90–0.98 and TiO_2 and Na_2O contents less than 0.4 wt% and 0.3 wt%, respectively. The Al_2O_3 contents vary from 0.5 to 5.2 wt% and tend to be higher in the inclusions in phlogopite and other silicates than the isolated phase in the matrix. The secondary diopside grains in marble (KST03) have purer endmember compositions than the primary grains in ACT01: X_{Mg} = 0.99–1.00, TiO_2< 0.1 wt%, Na_2O <0.1 wt%, and Al_2O_3 < 0.4 wt%. The primary diopside grains in the calc-silicate rock have lower X_{Mg} values (0.63–0.86: FeO = 4.6–11.7 wt%) and Al_2O_3 content (0.6–1.9 wt%) than those in the marble. TiO_2 and Na_2O contents are less than 0.3 wt% and 0.2 wt%, respectively.

4.8 | Other phases

The X_{Fe} [= $Fe^{3+}/(Fe^{3+} + Al)$] values of clinozoisite in a calc-silicate rock (KB01) are 0.06–0.18, and the MnO contents are less than 0.15 wt%. Titanite grains are relatively homogeneous and do not have distinct differences in compositions between inclusions and the matrix phases (KB01): Al_2O_3 = 2.4–2.8 wt%, Fe_2O_3 = 0.7 wt% and F = 0.55–0.83 wt% for the inclusion phase and Al_2O_3 = 2.3–2.9 wt%, Fe_2O_3 = 0.5–0.8 wt% and F = 0.39–0.65 wt% for the matrix phase. In the three calc-silicate rock samples, the Al_2O_3, Fe_2O_3, and F contents are 2.3–4.1 wt%, 0.2–0.8 wt%, and 0.7–1.1 wt%, respectively. Chlorine content is below the detection limit of 0.03 wt%.

5 | CALCITE–DOLOMITE SOLVUS GEOTHERMOMETER

Calcite-dolomite solvus thermometry was both experimentally and thermodynamically characterized by Anovitz and Essene (1987), Goldsmith and Newton (1969) and Powell, Condliffe and Condliffe (1984). As the calcite-dolomite solvus geothermometer is almost independent of pressure, it is known as a reliable thermometer for marble of amphibolite facies (e.g., Letargo, Lamb & Park, 1995; Rathmell, Streepey, Essene & van der Pluijm, 1999; Suzuki, 1977; Wada & Suzuki, 1983). However, Mg-rich calcite grains in granulite facies rocks typically show exsolution textures, suggesting re-equilibrium during the retrograde stage (e.g., Mizuochi, Satish-Kumar, Motoyoshi & Michibayashi, 2010).

Most calcite grains in the Mogok marble show exsolution textures and give re-equilibrated temperature conditions during retrograde stage of 350–610 °C for KST03, 370–540 °C for ZYK01 and 360–550 °C for OZ01, employing the calibration proposed by Anovitz and Essene (1987). However, some Mg-richer spots yield higher temperatures of 610–680 °C in ZYK01 (Figure 10b) and 600–660 °C in OZ01 (Figure 10c). The isolated calcite grains without exsolution textures in KST03 record low temperatures of 370–600 °C, similar to the exsolved inclusions (Figure 10a). The calcite replacing dolomite also shows temperatures of 400–580 °C. The isolated grains in ACT01, in contrast, show a continuous variation from 355 to 670 °C (Figure 10d), and inclusion calcite grains show lower temperature conditions of less than 410 °C.

The primary compositions of calcite grains estimated by reintegration of the exsolved calcite and dolomite aggregate yield higher and slightly scattered temperature ranges of 720–880 °C. In KST03, calcite grains included in clinohumite show distinctly higher temperature conditions (870–880 °C) than those in spinel (730–740 °C) (Figure 10a). In contrast, no distinct difference in temperature conditions owing to the difference of

modes of occurrence of calcite was observed in ZYK01 and OZ01. In ZYK01, the matrix calcite and the inclusion calcites in forsterite and spinel record temperatures of 745–760 °C, 735–760 °C, and 755–800 °C, respectively. In OZ01, calcite grains in the matrix and in spinel show temperature conditions of 720– 730 °C and 740–765 °C, respectively. In KST03 and ZYK01, isolated dolomite grains occur as a matrix phase and coexist with the exsolved calcite and dolomite aggregate. Therefore, the original Mg-richer calcite grains estimated for these samples have probably been in equilibrium with dolomite, which might represent the peak temperature conditions.

In OZ01, relatively coarse dolomite grains (up to 700–800 μm) occur in the matrix. However, they are probably coalescent phases of exsolution spherules as described in Section 3.2 (Figure 4c and d), and thus, the original Mg-richer calcite grains in OZ01 probably did not coexist with dolomite at the peak metamorphic stage. Therefore, temperature estimates of OZ01 (720–765 °C) based on the reintegrated Mg-rich calcite compositions probably define the lower limit of temperature conditions of the peak metamorphic stage. ACT01 contains no isolated dolomite in the matrix, and the matrix calcite grains showing temperatures up to 670 °C also define the minimum conditions of peak metamorphism. The minimum temperatures estimated by OZ01 and ACT01 are slightly lower than those estimated for the reintegrated compositions of KST03 and ZYK01 (730–880 °C).

Ye Kyaw Thu *et al*. (2016, 2017) estimated the equilibrium temperature conditions of paragneiss from the Onzon and Thabeikkyin areas as 780-860 °C at 0.60–0.84 GPa based on conventional geothermobarometers employing partial assemblages of Grt + Bt + Pl + Crd + Spl + Sill + Qz and empirical Ti-in-biotite and Zr-in-rutile geothermometers. Yonemura *et al*. (2013) also reported equilibrium conditions of

0.65–0.87 GPa/800–950 °C for garnet-orthopyroxene granulite samples in the Mogok area. The temperature conditions of metacarbonate rocks estimated by the calcite-dolomite geothermometer are consistent with those of the surrounding lithologies.

6 | DISCUSSION

6.1 | Peak equilibria and retrograde reactions

The relationships of *P-T*-fluid composition were calculated using THERMOCALC software ver. 3.33 (Powell & Holland, 1988) and an internally consistent thermodynamic data set (Holland & Powell, 1998; updated June 2009). Chemical compositions of minerals employed for the estimations of the metamorphic conditions are listed in Table 4. The activities of the solid solution phases are obtained from the following sources: scapolite, plagioclase, clinozoisite, diopside, and F-free tremolite (AX_2 program; http://www.esc.cam.ac.uk/research/research-groups/research-projects/tim-hollands-software-pages/ax), clinohumite (Rice, 1980), and F and Mg-rich tremolite in KST03 [$(1–X_F)^2$]] . Unit activity was used for other phases unless otherwise noted. The chemical formulae of minerals employed for reactions discussed on the following pages are after Holland and Powell (1998). The pressure condition at peak granulite facies stage was assumed to be 0.8 GPa, considering equilibrium conditions estimated for the paragneiss surrounding the marble and calc-silicate rock (Ye Kyaw Thu *et al*., 2016, 2017).

6.1.1 | CaO-MgO-SiO_2-H_2O-CO_2 system of marble

In KST03, F-bearing clinohumite occurs as a main constituent mineral and includes forsterite and calcite (Figure 3a and b). The assemblage of these phases is characteristically stable under high-temperature and F-bearing conditions (Rice, 1980; Satish-Kumar *et al.*, 2001). Figure 11 presents T–X_{CO2} diagrams showing the stability of these and related phases in the system CaO-MgO-SiO_2-CO_2-H_2O with excess calcite. Ba-rich phlogopite, pargasite/edenite, and spinel, which are major Al-bearing phases in KST03, have not been considered.

The sample KST03 contains dolomite as an isolated matrix phase, forsterite as an inclusion phase in clinohumite, and calcite as both the isolated matrix and inclusion phases. These textural relationships imply that forsterite, calcite and dolomite coexisted in equilibrium before and during the formation of clinohumite, and clinohumite formed by the following reaction:

$$4Fo + Dol + H_2O = Chu + Cal + CO_2. \qquad R1$$

This reaction would have resulted in a systematic increase of X_{CO2} along the univariant curve R1 with increasing temperature in a closed system. However, the limited occurrence of forsterite only as inclusions in clinohumite (Figure 3a and b) implies that forsterite was not in equilibrium with dolomite and the inclusion + host assemblage of Chu + Fo + Cal was stable at the peak metamorphic stage. The stability field of this assemblage is defined by the combination of reaction R1 and the following reaction:

$$14Fo + Cal + 3H_2O = 3Chu + Di + CO_2 . \qquad R2$$

The matrix assemblage of clinohumite + calcite + dolomite was also stable under the estimated peak metamorphic condition (Fig. 11a). These facts imply that the X_{CO2} value of fluid was firstly internally buffered by the reaction R1, and thus, probably increased with increasing temperature at the beginning of clinohumite formation, but subsequently

decreased, which destabilized the Fo + Dol assemblage, at the peak metamorphic stage, although the mechanism of the change in fluid composition remains to be explained. The lower temperature and X_{CO2} limits of the Chu + Fo + Cal assemblage are estimated as about 810 °C and 0.60 for KST03 (invariant point [Tr] in Figure 11a).

A zone consisting of dolomite and a symplectitic aggregate of tremolite and dolomite constantly develops between the clinohumite and matrix calcite (Figure 3a and b), although retrograde diopside rimmed by tremolite rarely joins the aggregate (Figure 3a and e). The common occurrence of diopside-free tremolite and dolomite symplectite suggests that the following reaction mainly controlled the breakdown of the Chu + Cal assemblage during the retrograde stage:

$$2Chu + 15Cal + 11CO_2 \rightarrow Tr + 13Dol + H_2O \qquad R3$$

However, this reaction is metastable for a wide range of X_{CO2} conditions, at least > 0.001, under the higher pressure of > 0.7 GPa, thus an alternative reaction R4, controls the stability of the Chu + Cal assemblage under the assumed wide X_{CO2} conditions (Figure 11a):

$$Chu + 9Cal + 5CO_2 \rightarrow 2Di + 7Dol + H_2O \qquad R4$$

The rare occurrence of diopside replaced by tremolite in the aggregate of tremolite and dolomite (Figure 3e) probably implies that the reaction R4 progressed locally before proceeding to the reaction R3. The reaction R3 is stable under lower pressure of < 0.7 GPa and X_{CO2} conditions, and its upper stability is defined by the invariant point [Fo], which shifts from 0.002/490 °C at 0.65 GPa, through 0.084/620 °C at 0.5 GPa, to 0.25/640 °C at 0.4 GPa with decreasing pressure (Figure 11b). This fact suggests that the reaction between clinohumite and calcite shown in Figure 3a, b, and f have

progressed during the retrograde stage under distinctly lower X_{CO2} conditions than during the peak metamorphic stage.

ZYK01 is composed of forsterite, calcite, and dolomite without diopside. The stability of this assemblage is defined by the combination of reaction R1 and the following reaction.

$$\text{Di} + 3\text{Dol} = 2\text{Fo} + 4\ \text{Cal} + 2\text{CO}_2 \qquad \text{R5}$$

The Fo + Cal + Dol assemblage is stable at higher X_{CO2} conditions than the Chu + Fo + Cal assemblage observed in KST03 for the same compositional conditions (cf., Figure 11a). Its stability field, however, shifts towards lower temperature and X_{CO2} conditions with increasing activity, decreasing X_F, of clinohumite. For example, X_{CO2} and temperature conditions of the invariant point [Tr] for X_F *(Chu)* = 0.5 are 0.004 and 530 °C, respectively, at 0.8 GPa. Therefore, these two assemblages may have shared the same temperature and X_{CO2} conditions, if the F content of the metamorphic fluid of ZYK01 were relatively lower than that of KST03. The lower limit of the X_{CO2} condition for the stability of Fo + Cal + Dol assemblage cannot be estimated because of the absence of clinohumite in ZYK01. However, this assemblage in ZYK01 does not conflict with the high temperature and X_{CO2} estimates of the peak metamorphic stage for KST03, which was collected from the Kyetsaung Taung marble unit, as was ZYK01 (Figure 2b). In ZYK01, the coexisting forsterite, calcite, and dolomite do not show any reaction such as R5 during the retrograde stage. This might imply that the X_F value of metamorphic fluid of ZYK01 was lower than that of KST03 even during the retrograde stage, and thus: the stability field of the clinohumite-bearing assemblage reduced and that of the Fo + Cal + Dol assemblage relatively expanded towards lower X_{CO2} and temperature conditions; and the X_{CO2} value was relatively low during the retrograde

stage, for example, the Fo + Cal + Dol assemblage is stable under $X_{CO2} > 0.05$ at 0.5 GPa/600 °C for X_F *(Chu)* = 0.5. The silicate mineral-free assemblage in the CaO–MgO-SiO_2 system of OZ01 and Di + Cal assemblage of ACT01 are also stable under the high temperature and X_{CO2} conditions during granulite facies stage deduced from the mineral assemblages of KST03 and ZYK01 (Figure 11a).

6.1.2 | CaO-MgO-Al_2O_3-SiO_2-H_2O-CO_2 system of calc-silicate rock

The characteristic mineral assemblages of the calc-silicate rock at the peak granulite facies stage are Scp + Pl + Di + Qz + Cal for WBY01 and Scp + Di + Qz + Cal for OZ03 and KB01. Figure 12 shows T–X_{CO2} diagram that demonstrate the stability of scapolite and related phases of WBY01 and OZ03 in the CaO-Al_2O_3-SiO_2-CO_2-H_2O system with excess quartz and calcite. Figure 13 shows T–X_{CO2} diagrams of scapolite and related phases of KB01 in the CaO-MgO-Al_2O_3-SiO_2-CO_2-H_2O system during the peak granulite facies and the retrograde stage.

The peak metamorphic conditions of the scapolite-bearing calc-silicate rock are defined by the following reactions:

$$3An + Cal = Mei \qquad R6$$

$$Mei + 3Qz + 5Cal = 3Grs + 6CO_2 \qquad R7$$

$$Qz + Cal = Wo + CO_2 \qquad R8$$

Temperature and X_{CO2} conditions of the invariant points defined by these reactions calculated employing unit activity for grossular ([Wo] and [Wo, Czo] in Figures 12 and 13, respectively)are 795 °C/0.22, 780 °C/0.17, and 790 °C/0.19 for WBY01, OZ03, and KB01, respectively. The invariant point [Wo] shifts towards higher X_{CO2} conditions under constant temperature with decreasing grossular composition of garnet in the

system (Figure 12), and thus, the isobaric diagram calculated assuming unit activity of grossular defines the minimum X_{CO2} condition. Therefore, temperature and X_{CO2} conditions at the peak metamorphic stage of WBY01, which contains a Scp + Pl + Qz + Cal assemblage, were estimated as 795 °C and > 0.22, respectively, at P = 0.8 GPa (Figure 12). Conversely, OZ03 and KB01 contain no prograde plagioclase, and thus, the Scp + Qz + Cal assemblage defines the minimum temperature and X_{CO2} conditions of 780 °C and 0.17 for OZ03 (Figure 12) and 790 °C and 0.19 for KB01 (Figure 13a), respectively, at P = 0.8 GPa. These estimates of the lower limit conditions are consistent with the estimates by the Scp + Pl + Qz + Cal equilibrium for WBY01.

In KB01, clinozoisite occurs forming aggregate with quartz and calcite, and thus, the retrograde trajectory might have passed the stability field of the Czo + Qz + Cal assemblage defined by the following reactions R9 and R10:

$$2Czo + 3Qz + 5Cal = 3Grs + H_2O + 5CO_2 \qquad R9$$

$$2Czo + CO_2 = 3An + Cal + H_2O \qquad R10$$

This stability field is located at lower temperature and expands towards lower X_{CO2} condition than that of the Scp + Qz + Cal assemblage under the same pressure, and shifts towards lower temperature condition with decreasing pressure (Figure 13a). In Figure 13a, the reactions R9 was calculated assuming pure grossular composition, and the univariant line R9 and invariant point [Mei, Wo] shift toward lower temperature and higher X_{CO2} conditions with decreasing activity of grossular. Therefore, the stability field of the Czo + Qz + Cal assemblage in Figure 13a defined by the combination of reactions R9 and R10 shows the maximum temperature and minimum X_{CO2} value of the stability of clinozoisite in the calc-silicate rock (KB01). Additionally, diopside occurs coexisting with the Czo + Qz + Cal assemblage without tremolite, suggesting that the

temperature and X_{CO2} conditions of the Czo + Di + Qz + Cal assemblage's stability were defined by the combination of R9, R10 and the following reaction:

$$Tr + 2Qz + 3Cal = 5Di + H_2O + 3CO_2 \qquad R11$$

Consequently, the temperature and X_{CO2} of the main retrograde stage based on the stability of the Czo + Di + Qz + Cal assemblage are estimated at < 620 °C and < 0.155 at P = 0.5 GPa, respectively (Figure 13a).

In KB0, clinozoisite also occurs replacing scapolite (Figure 5c), implying the possible following retrograde reaction:

$$Mei + H_2O \rightarrow Czo + CO_2 \qquad R12$$

This reaction is stable only in quartz-absent metacarbonate rock, because, in the quartz-excess system, the stability of scapolite is defined by reactions R6 and R7, and that of clinozoisite is controlled by alternative reactions R9 and R10 as discussed above (Figure 13a). Figure 13b shows stability of the reaction R12 in the quartz-free system. An invariant point [Grs, Wo], including reaction R12, is located at high temperature/low X_{CO2} conditions of 750 °C/0.059 for P = 0.8 GPa and almost isothermally decreases with decreasing pressure down to 745°C/0.009 at P = 0.4 GPa (Figure 13b). These metamorphic conditions imply that wollastonite should have been stable instead of Qz + Cal assemblage (R8) if the reaction R12 has stably progressed during the retrograde stage. However, the wide occurrence of Qz + Cal assemblage and absence of wollastonite in metacarbonate rocks throughout the studied Onzon–Thabeikkyin region are inconsistent with the temperature and X_{CO2} conditions supposed by the reaction R12. Consequently, the replacement of scapolite by clinozoisite in KB01 might have not progressed in stable under the high temperature and low X_{CO2} conditions in the

SiO_2-undersaturated system, and probably suggests metastable reaction in the stability field of Qz + Cal assemblage.

In a calc-silicate rock (WBY01), scapolite grains were replaced by plagioclase and calcite with small amounts of quartz (Figure 5b), which follows reaction R6. If the quartz grains were a breakdown product of scapolite, the following reaction might be more suitable, as discussed by Motoyoshi et al. (1991):

$$\text{Scp} \rightarrow \text{Pl} + \text{Qz} + \text{Cal} \qquad \text{R13}$$

They considered that the precipitation of quartz is due to a small excess of SiO_2 in the scapolite over the ideal composition, or, alternatively, SiO_2 was released together with Na_2O from the marialite component.

6.2 | Evolution of metamorphic fluids

Figure 14 summarizes the *P-T* conditions of the peak granulite facies and subsequent low-amphibolite facies stage, and compares the compositions of metamorphic fluids of the marble and the calc-silicate rock of the Mogok metamorphic belt between the two stages of recrystallizations. Low X_{CO2} fluid composition of paragneiss surrounding the metacarbonate rocks, which is inferred based on their carbonate minerals-absent assemblages (Maw Maw Win *et al*., 2016; Ye Kyaw Thu *et al*., 2016, 2017), was also shown for comparison.

6.2.1 | Peak granulite facies stage

The mineral assemblages of the metacarbonate rocks in the Onzon–Thabeikkyin region recorded the minimum temperature conditions of 780–810 °C at 0.8 GPa for the peak metamorphic stage. The calcite-dolomite solvus geothermometer also suggested a

minimum temperature of 720–765 °C and possible equilibrium temperature up to 870–880 °C. These estimates are consistent with those for peak granulite facies metamorphism recorded in the paragneiss of the Onzon–Thabeikkyin region (0.60–0.84 GPa/780–860 °C) (Ye Kyaw Thu *et al.*, 2016, 2017). These data suggest that the metacarbonate rocks and the surrounding paragneiss shared similar *P-T* metamorphic conditions with the granulite facies. However, fluid compositions at the peak metamorphic stage seem to have been different among the lithologies. The X_{CO2} values of the metamorphic fluid were significantly higher (> 0.60 in the marble and > 0.17–0.22 in the calc-silicate rock) than that of a nearly pure H_2O-fluid inferred for the paragneiss. Although it is not conclusive that the X_{CO2} values were different between the marble and calc-silicate rock at peak metamorphic stage, there were significant discontinuities in the metamorphic fluid compositions between the metacarbonate rocks and paragneiss.

6.2.2 | Retrograde stage

The recrystallization textures of granulite facies assemblages (Figures 3a, b, e, and f and 5c) during the retrograde stage imply that the X_{CO2} values of the metamorphic fluid decreased with decreasing metamorphic *P-T* conditions. For the discussions of temperature and X_{CO2} conditions during retrograde recrystallization, the pressure was assumed to be 0.5 GPa because the paragneiss in the Onzon–Thabeikkyin region were extensively recrystallized at P = 0.40–0.55 GPa with fluid infiltration (Ye Kyaw Thu *et al.*, 2016, 2017).

The retrograde reaction between clinohumite and calcite (reaction R3) observed in the marble (KST03) probably progressed at X_{CO2} and temperature conditions lower than

0.084 and 620 °C at $P = 0.5$ GPa, respectively (Figure 11b). The stability of Fo + Cal + Dol assemblage without Di throughout the peak and retrograde metamorphic stages in ZYK01 also suggest decrease of X_{CO2} condition with decreasing temperature as discussed in section 6.1.1. The coexisting clinozoisite, diopside, quartz, and calcite of KB01 estimate the X_{CO2} and temperature conditions as < 620 °C and < 0.155 at $P = 0.5$ GPa, respectively (Figure 13a), also suggesting lower X_{CO2} condition at retrograde stage than that at the peak granulite facies stage.

Consequently, the metacarbonate rocks studied herein recorded a distinct gap of fluid composition between the peak and retrograde stages (Figure 14). Ye Kyaw Thu *et al.* (2016, 2017) suggested that the Mogok paragneiss in the Onzon area have recrystallized to varying degree with extensive infiltration of H_2O-rich fluids during exhumation (0.40–0.55 GPa/620–640 °C). A similar extensive hydration stage was also recorded in the paragneiss from the Mandalay region (0.3-0.5 GPa/600–680 °C) by Maw Maw Win *et al.* (2016) and Enami, Nagaya and Maw Maw Win (2017). Although there is no conclusive evidence suggesting that the retrograde recrystallizations of the metacarbonate rocks developed under conditions similar to those of the paragneiss, there is no inconsistency in the P–T estimations of the retrograde stage between the two lithologies. Episodic infiltration of H_2O-rich fluid during exhumation probably enabled the retrograde reactions of the metacarbonate rocks with low X_{CO2}-fluid phases under low-amphibolite facies conditions.

6.3 | Contrasts in fluid compositions

The metamorphic fluid of the Mogok metacarbonate rocks had distinctly higher X_{CO2} composition than the H_2O-dominant fluid of the paragneiss at the peak metamorphic

stage. There might have also been X_{CO2} contrast between the marble and calc-silicate rock. Yui, Zaw and Wu (2008) analysed $\delta^{13}C$–$\delta^{18}O$ compositions of ruby-bearing and related marble from the Mogok metamorphic belt, and concluded that the formation of ruby might have resulted from CO_2-rich fluid–rock interaction, while spinel- and forsterite-bearing marble was genetically recrystallized under low X_{CO2} environment. Some major constituent minerals in the marble and calc-silicate rock are richer in F and Cl, respectively. The mafic minerals in the marble have nearly Mg-endmember compositions (X_{Mg} = 0.92–1.00) and those in the calc-silicate rock are more enriched in FeO (X_{Mg} = 0.63–0.86 for diopside). Therefore, the distinct differences of halogen compositions were certainly controlled by the Fe-F and Mg-Cl avoidance principles. However, the halogen compositions of minerals also reflected the characteristics of the fluid compositions and probably indicate the contrast of the halogen compositions of metamorphic fluids during the peak granulite facies stage between these metacarbonate lithologies. These features suggest that the metamorphic fluid compositions were internally buffered and the effective migration of metamorphic fluids, which causes extensive change in the fluid compositions beyond the major lithologic boundaries, did not occur during the peak granulite facies stage throughout the Mogok metamorphic belt.

Similar local fluid buffering during peak metamorphism was well documented in metacarbonate rocks from many granulite facies terranes (e.g., Kaneko et al., 2005; Satish-Kumar et al., 1996; Satish-Kumar et al., 2001). These studies also concluded that X_{CO2} values of the metamorphic fluids were probably maintained as high as 0.5–0.8 even during the low-granulite and amphibolite facies stages of the retrograde stage. In contrast, in the case of the Mogok metamorphic belt, the far-ranging infiltration of

H_2O-rich fluids during exhumation and hydration stage probably decreased the X_{CO2} value of the metacarbonate rocks and extensively homogenized the metamorphic fluid compositions throughout the metacarbonate rocks and the surrounding paragneiss. Maw Maw Win et al. (2016) discussed the relationship between the chemical zoning of monazite and CHIME ages of each zone in a Mogok paragneiss, and considered that the monazite ages were reset to a varying degree at ca. 24 Ma due to fluid infiltration. In the Mogok metamorphic belt, extensive acidic magmatic intrusions were reported during late Oligocene-early Miocene by zircon U-Pb ages (e.g., Barleyet al., 2003; Mitchell, Chung, Thura Oo, Lin and Hung, 2012; Searle et al., 2007). Although the origin of the inferred H_2O-dominant fluid during the exhumation has not been conclusively established, released fluid from the intruded and solidified melt might have contributed to the modification of the fluid composition. Alternatively, the fluid might have been released from a slab dehydrated during active subduction.

7 | SUMMARY

The following points summarize this study of the metacarbonate rocks from the Mogok metamorphic belt:

1 The metacarbonate rocks from the middle segment of the Mogok metamorphic belt studied are grouped into the dolomite-bearing and quartz-free marble and the dolomite-free and quartz-bearing calc-silicate rock. The halogen contents of minerals show distinct contrast between the marble and calc-silicate rock. Hydrous phases in marble are characteristically rich in F: clinohumite up to 4.1 wt%, phlogopite up to 3.6 wt%, prograde amphibole up to 2.5 wt%, and retrograde amphibole up to 1.5 wt%. In contrast, calc-silicate rock is not composed of a F-bearing phase and

scapolite grains characteristically contain Cl up to 0.5 wt% in the prograde phase and 3.1 wt% in the retrograde phase. Some phlogopite grains in marble have unusually high BaO and Na_2O contents of up to 7.9 wt% and 1.4 wt%, respectively.

2 Thermodynamic analyses of reaction relations of minerals show that the metacarbonate rocks were equilibrated under high temperature conditions of > 780–810 °C at 0.8 GPa, which are equivalent to the surrounding paragneiss. However, X_{CO2} values of metamorphic fluids of the metacarbonate rocks during the peak granulite facies stage were distinctly higher than those of the surrounding paragneiss: $X_{CO2} > 0.6$ for marble and > 0.17–0.22 for calc-silicate rock. The high X_{CO2} compositions during the prograde stage decreased to $X_{CO2} < 0.08$ for marble and < 0.155 for calc-silicate rock at around 0.5 GPa/600 °C during retrograde stage.

3 The differences in halogen compositions of constituent minerals and the estimated X_{CO2} values of metamorphic fluids between the marble and calc-silicate rock imply that compositions of metamorphic fluids during the granulite facies stage were internally buffered. Migration of these fluids, which effectively caused inhomogeneity in the composition, did not progress beyond the lithological boundaries among these metacarbonate rocks and the surrounding paragneiss. Subsequently, the fluid compositions were extensively homogenized and became low X_{CO2} during the retrograde stage by infiltration of H_2O-rich fluids. The hydrous fluids probably originated from one or both of the following sources: (1) fluids released from acidic melts that intruded at a later stage of metamorphism; and/or (2) dehydration of a slab undergoing subduction.

ACKNOWLEDGEMENTS

The authors thank members of the petrology group at Nagoya University for numerous discussions and comments, and M. Tsuboi for his help and discussion during fieldwork. Valuable and constructive comments by two reviewers A. Proyer and anonymous one and editor D. Whitney greatly helped to improve this manuscript. Sincere thanks are extended to the late Myint Lwin Thein and his research colleagues for allowing us to cite their unpublished field data. This research was partially supported by a scholarship (YKT) from the Ministry of Education, Culture, Sports, Science, and Technology (MEXT), Japan and by Grants-in-Aid for Scientific Research (ME, 25400511 and 17K05705) from the Japan Society for the Promotion of Science (JSPS).

REFERENCES

Acharyya, S.K. (2007). Collisional emplacement history of the Naga-Andaman ophiolites and the position of the eastern Indian suture. *Journal of Asian Earth Sciences*, *29*, 229-242.

Anovitz, L.M., & Essene, E.J. (1987). Phase equilibria in the system $CaCO_3$-$MgCO_3$-$FeCO_3$. *Journal of Petrology*, *28*, 389-414.

Barber, A.J., & Crow, M.J. (2009). Structure of Sumatra and its implications for the tectonic assembly of Southeast Asia and the destruction of Paleotethys. *Island Arc*, *18*, 3-20.

Barley, M.E., Pickard, A.L., Khin Zaw, Rak, P., & Doyle, M.G. (2003). Jurassic to Miocene magmatism and metamorphism in the Mogok metamorphic belt and the India-Eurasia collision in Myanmar. *Tectonics*, *22*, 1–11, doi.10.1029/2002TC001398.

Bertrand, G., Rangin, C., Maluski, H., & Bellon, H. (2001). Diachronous cooling along the Mogok metamorphic belt (Shan Scarp, Myanmar); the trace of the northward migration of the Indian syntaxis. *Journal of Asian Earth Sciences*, *19*, 649-659.

Bertrand, G., Rangin, C., Maluski, H., Tin Aung Han, Ohn Myint, Win Maw, ... San Lwin (1999). Cenozoic metamorphism along the Shan Scarp (Myanmar); evidences for ductile shear along the Sagaing Fault or the northward migration of the eastern Himalayan syntaxis? *Geophysical Research Letters*, *26*, 915-918.

Bose, S., Das, K., & Fukuoka, M. (2005). Fluorine content of biotite in granulite-grade metapelitic assemblages and its implications for the Eastern Ghats granulites. *European Journal of Mineralogy*, *17*, 665-674.

Boucot, A.J. (2002). Some thoughts about the Shan-Thai terrane. In: *Proceedings of the Symposium on Geology of Thailand. Department of Mineral Resources* (eds Mantajit, N. & Potisat, S.), p. 26-31: Bangkok.

Buick, I.S., Cartwright, I., & Williams, I.S. (1997). High-temperature retrogression of granulite-facies marbles from the Reynolds Range Group, central Australia; phase equilibria, isotopic resetting and fluid fluxes. *Journal of Petrology*, *38*, 877-910.

Carmichael, D.M. (1970). Intersecting isograds in the Whetstone Lake area, Ontario. *Journal of Petrology*, *11*, 147-181.

Connolly, J.A.D., & Trommsdorff, V. (1991). Petrogenetic grids for metacarbonate rocks; pressure-temperature phase-diagram projection for mixed-volatile systems. *Contributions to Mineralogy and Petrology*, *108*, 93-105.

Dasgupta, S. (1993). Contrasting mineral parageneses in high-temperature calc- silicate granulites; examples from the Eastern Ghats, India. *Journal of Metamorphic Geology*, 11, 193-202.

Enami, M., Nagaya, T., & Maw Maw Win (2017). An integrated EPMA-EBSD study of metamorphic histories recorded in garnet. *American Mineralogist*, *101*, 192-204.

Evans, B.W., Shaw, D.M., & Haughton, D.R. (1969). Scapolite Stoichiometry. *Contributions to Mineralogy and Petrology*, *24*, 293-305.

Faryad, S.W. (2002). Metamorphic conditions and fluid compositions of scapolite-bearing rocks from the Lapis Lazuli deposit at Sare Sang, Afghanistan. *Journal of Petrology*, *43*, 725-747.

Ferry, J.M. (1994). A historical review of metamorphic fluid flow. *Journal of Geophysical Research*, *99*, 15487-15498.

Fleet, M.E. (2003). Sheet silicates: Mica. Rock-Forming Minerals, The Geplogical Society: London. 758 pp.

Gallien, F., Mogessie, A., Bjerg, E., Delpino, S., & de Machuca, B.C. (2009). Contrasting fluid evolution of granulite-facies marbles: implications for a high-T intermediate-P terrain in the Famatinian Range, San-Juan, Argentina. *Mineralogy and Petrology*, *95*, 135-157.

Gardiner, N.J., Robb, L.J., Morley, C.K., Searle, M.P., Cawood, P.A., Whitehouse, M.J., … Tin Aung Myinth (2016). The tectonic and metallogenic framework of Myanmar: A Tethyan mineral system. *Ore Geology Reviews*, *79*, 26-45.

Gardiner, N.J., Searle, M.P., Robb, L.J., & Morley, C.K. (2015). Neo-Tethyan magmatism and metallogeny in Myanmar - An Andean analogue? *Journal of Asian Earth Sciences*, *106*, 197-215.

Garnier, V., Maluski, H., Giuliani, G., Ohnenstetter, D., & Schwarz, D. (2006). Ar-Ar and U-Pb ages of marble-hosted ruby deposits from Central and Southeast Asia. *Canadian Journal of Earth Sciences*, *43*, 509-532.

Gaspar, J.C. (1992). Titanian clinohumite in the carbonatites of the Jacupiranga Complex, Brazil; mineral chemistry and comparison with titanian clinohumite from other environments. *American Mineralogist*, *77*, 168-178.

Ghose, N.C., Chatterjee, N., & Fareeduddin (2013). A Petrographic Atlas of Ophiolite: An example from the eastern India-Asia Collision Zone, Springer 234 pp.

Goldsmith, J.R., & Newton, R.C. (1969). P-T-X relations in the system $CaCO_3$ -$MgCO_3$ at high temperatures and pressures. *American Journal of Science*, *267-A*, 160-190.

Harley, S.L., Fitzsimons, I.C.W., & Buick, I.S. (1994). Reactions and textures in wollastonite-scapolite granulites and their significance for pressure-temperature-fluid histories of high-grade terranes. *Precambrian Research*, *66*, 309-323.

Higashino, F., Kawakami, T., Satish-Kumar, M., Ishikawa, M., Maki, K., Tsuchiya, N., … Hirata, T. (2013). Chlorine-rich fluid or melt activity during granulite facies metamorphism in the Late Proterozoic to Cambrian continental collision zone-An example from the Sor Rondane Mountains, East Antarctica. *Precambrian Research*, *234*, 229-246.

Holland, T.J.B., & Powell, R. (1998). An internally consistent thermodynamic data set for phases of petrological interest. *Journal of Metamorphic Geology*, 16, 309-343.

Jones, N.W., Ribbe, P.H., & Gibbs, G.V. (1969). Crystal chemistry of humite minerals. *American Mineralogist*, *54*, 391-411.

Kaneko, Y., Miyano, T. & Tsunogae, T. (2005). Fluid compositions and local fluid buffering during the retrograde metamorphism of Al-bearing dolomitic calc-silicate granulites in the Limpopo Central Zone, southern Africa. *Journal of African Earth Sciences*, *41*, 61-77.

Kato, T. (2005). New accurate Bence-Albee α-factors for oxides and silicates calculated from the PAP correction procedure. *Geostandrds and Geoanalytical Research*, *29*, 83-94.

Leake, B.E., Woolley, A.R., Arps, C.E.S., Birch, W.D., Gilbert, M.C., Grice, J.D., … Guo, Y.Z. (1997). Nomenclature of amphiboles: Report of the subcommittee on

amphiboles of the International Mineralogical Association, commission on new minerals and mineral names. *American Mineralogist*, *82*, 1019-1037.

Letargo, C.M.R., Lamb, W.M., & Park, J.S. (1995). Comparison of calcite + dolomite thermometry and carbonate + silicate equilibria: Constraints on the conditions of metamorphism of the Llano uplift, central Texas, U.S.A. *American Mineralogist*, *80*, 131-143.

Maw Maw Win, Enami, M., & Kato, T. (2016). Metamorphic conditions and CHIME monazite ages of Late Eocene to Late Oligocene high-temperature Mogok metamorphic rocks in central Myanmar. *Journal of Asian Earth Sciences*, *117*, 304-316.

Maw Maw Win, Enami, M., Kato, T., & Ye Kyaw Thu (2017 in press). A mechanism for Nb incorporation in rutile and application of Zr-in-rutile thermometry: A case study from granulite facies paragneisses of the Mogok metamorphic belt, Myanmar. *Mineralogical Magazine*, *81*, 1503-1521.

Metcalfe, I. (1988). Origin and assembly of south-east Asian continental terranes. In: *Gondwana and Tethys* (eds Audley-Charles, M.G. & Hallam, A.) *Geological Society Special Publications*, p. 101-118, Blackwell Scientific Publications: Oxford.

Metcalfe, I. (2000). The Bentong–Raub Suture Zone. *Journal of Asian Earth Sciences*, *18*, 691-712.

Mitchell, A., Chung, S.L., Thura Oo, Lin, T.H., & Hung, C.H. (2012). Zircon U-Pb ages in Myanmar: Magmatic-metamorphic events and the closure of a neo-Tethys ocean? *Journal of Asian Earth Sciences*, *56*, 1-23.

Mitchell, A.H.G. (1977). Tectonic settings for emplacement of Southeast Asian tin granites. *Bulletin of Geological Society of Malaysia*, *9*, 123-140.

Mitchell, A.H.G. (1993). Cretaceous–Cenozoic tectonic events in the western Myanmar (Burma)–Assam region. *Journal of Geological Society*, *150*, 1089-1102.

Mitchell, A.H.G., Myint Thein Htay, Kyaw Min Htun, Myint Naing Win, Thura Oo, & Tin Hlaing (2007). Rock relationships in the Mogok metamorphic belt, Tatkon to Mandalay, central Myanmar. *Journal of Asian Earth Sciences*, *29*, 891-910.

Mizuochi, H., Satish-Kumar, M., Motoyoshi, Y., & Michibayashi, K. (2010). Exsolution of dolomite and application of calcite-dolomite solvus geothermometry in high-grade marbles: an example from Skallevikshalsen, East Antarctica. *Journal of Metamorphic Geology*, *28*, 509-526.

Moecher, D.P., & Essene, E.J. (1990). Scapolite phase equilibria: additional constraints on the role of CO_2 in granulite genesis. In: *Granulites and Crustal Evolution* (eds Vielzeuf, D. & Vidal, P.) *NATO Science Series, Series C: Mathematical and Phy*sical Sciences, p. 385-396, Springer: Netherlands.

Montel, J.-M., Kato, T., Enami, M., Cocherie, A., Finger, F., Williams, M., … Jercinovic, M. (2018). Electron-microprobe dating of monazite: The story. Chemical Geology, doi: 10.1016/j.chemgeo.2017.11.001.

Motoyoshi, Y., & Hensen, B.J. (2001). F-rich phlogopite stability in ultra-high-temperature metapelites from the Napier Complex, East Antarctica. *American Mineralogist*, *86*, 1404-1413.

Motoyoshi, Y., Thost, D.E., & Hensen, B.J. (1991). Reaction textures in calc-silicate granulites from the Bolingen Islands, Prydz Bay, East Antarctica; implications for the retrograde P-T path. *Journal of Metamorphic Geology*, *9,* 293-300.

Myint Lwin Thein, Ohm Myint, Sun Kyi, & Hpone Myint Win (1990). Geology and stratigraphy of the metamorphosed Early Paleozoic rocks of the Mogok-Thabeikkyin-Singu-Madaya areas. Unpublished staff report. 24 pp.

Pan, Y., & Fleet, M.E. (1996). Rare earth element mobility during prograde granulite facies metamorphism; significance of fluorine. *Contributions to Mineralogy and Petrology*, *123*, 251-262.

Paquette, J., & Reeder, R.J. (1990). Single-crystal X-ray structure refinements of two biogenic magnesian calcite crystals. *American Mineralogist*, *75*, 1151-1158.

Pattison, D.R.M. (2001). Instability of Al_2SiO_5 "triple-point" assemblages in muscovite+biotite+quartz-bearing metapelites, with implications. *American Mineralogist*, *86*, 1414-1422.

Piazolo, S., & Markl, G. (1999). Humite- and scapolite-bearing assemblages in marbles and calcsilicates of Dronning Maud Land, Antarctica; new data for Gondwana reconstructions. *Journal of Metamorphic Geology*, *17*, 91-107.

Powell, R., Condliffe, D.M., & Condliffe, E. (1984). Calcite-dolomite geothermometry in the system $CaCO_3$-$MgCO_3$-$FeCO_3$: an experimental study. *Journal of Metamorphic Geology*, *2*, 33-41.

Powell, R., & Holland, T.J.B. (1988). An internally consistent dataset with uncertainties and correlations: 3. Applications to geobarometry, worked examples and a computer program. *Journal of Metamorphic Geology*, *6*, 173-204.

Rathmell, M.A., Streepey, M.M., Essene, E.J., & van der Pluijm, B.A. (1999). Comparison of garnet-biotite, calcite-graphite, and calcite-dolomite thermometry in the Grenville Orogen; Ontario, Canada. *Contributions to Mineralogy and Petrology*, *134*, 217-231.

Rice, J.M. (1980). Phase equilibria involving humite minerals in impure dolomitic limestones; Part I, Calculated stability of clinohumite. *Contributions to Mineralogy and Petrology*, *71*, 219-235.

Ridd, M.F., & Watkinson, I. (2013). The Phuket-Slate Belt terrane: tectonic evolution and strike-slip emplacement of a major terrane on the Sundaland margin of Thailand and Myanmar. *Proceedings of the Geologists' Association*, *124*, 994-1010.

Satish-Kumar, M., & Harley, S.L. (1998). Reaction textures in scapolite-wollastonite-grossular calc-silicate rock from the Kerala khondalite belt, southern India; evidence for high-temperature metamorphism and initial cooling. *Lithos*, *44*, 83-99.

Satish-Kumar, M., Hermann, J., Tsunogae, T., & Osanai, Y. (2006). Carbonation of Cl-rich scapolite boudins in Skallen, East Antarctica; evidence for changing fluid condition in the continental crust. *Journal of Metamorphic Geology*, 24, 241-261.

Satish-Kumar, M., & Niimi, N. (1998). Fluorine-rich clinohumite from Ambasamudram marbles, southern India; mineralogical and preliminary FTIR spectroscopic characterization. *Mineralogical Magazine*, *62*, 509-519.

Satish-Kumar, M., Santosh, M., Harley, S.L., & Yoshida, M. (1996). Calc-silicate assemblages from the Kerala Khondalite Belt, southern India: Implications for pressure-temperature-fluid histories. *Journal of Southeast Asian Earth Sciences*, *14*, 245-263.

Satish-Kumar, M., Wada, H., Santish, M., & Yoshida, M. (2001). Fluid-rock history of granulite facies humite-marbles from Ambasamudram, southern India. *Journal of Metamorphic Geology, 19*, 395-410.

Schneider, C.A., Rasband, W.S., & Eliceiri, K.W. (2012). NIH Image to ImageJ: 25 years of image analysis. *Nature Methods*, *9,* 671-675.

Searle, M.P., Noble, S.R., Cottle, J.M., Waters, D.J., Mitchell, A.H.G., Tin Hlaing, … Horstwood, M.S.A. (2007). Tectonic evolution of the Mogok metamorphic belt, Burma (Myanmar) constrained by U-Th-Pb dating of metamorphic and magmatic rocks. *Tectonics*, *26*, TC3014, doi.10.1029/2006TC002083.

Suwa, K., Enami, M., & Horiuchi, T. (1987). Chlorine-rich potassium hastingsite from West Ongul island, Lützow-Holm bay, east Antarctica. *Mineralogical Magazine*, *51*, 709-714.

Suzuki, K. (1977). Local equilibrium during the contact metamorphism of siliceous dolomites in Kasuga-mura, Gifu-ken, Japan. *Contributions to Mineralogy and Petrology*, *61*, 79-89.

Suzuki, K. & Adachi, M. (1991). Precambrian provenance and Silurian metamorphism of the Tsubonosawa paragneiss in the South Kitakami terrane, Northeast Japan, revealed by the chemical Th-U-total Pb isochron ages of monazite, zircon and xenotime. *Geochemical Journal*, *25*, 357-376.

Tsunogae, T., Hokada, T., Crowe, W.A., Osanai, Y., Owada, M., & Toyoshima, T. (2003). High fluorine pargasites in ultrahigh temperature granulites from Tonagh Island in the Archean Napier Complex, East Antarctica. *Lithos*, *70,* 21-38.

Valley, J.W. (1986). Stable isotope geochemistry of metamorphic rocks. In: *Stable Isotopes in High Temperature Geological Processes* (eds Valley, J.W., Taylor, J., H.P. & O'Neil, J.R.) *Reviews in Mineralogy*, p. 445-490, Book Crafters, Inc.: Chelsea, Michigan.

Wada, H., & Suzuki, K. (1983). Carbon isotopic thermometry calibrated by dolomite-calcite solvus temperatures. *Geochimica et Cosmochimica Acta*, *47*, 697-706.

Warren, R.G., Hensen, B.J., & Ryburn, R.J. (1987). Wollastonite and scapolite in Precambrian calc-silicate granulites from Australia and Antarctica. *Journal of Metamorphic Geology*, *5*, 213-223.

White, T.J., & Hyde, B.G. (1982). Electron microscope study of the humite minerals: I. Mg-rich specimens. *Physics and Chemistry of Minerals*, *8*, 55-63.

Whitney, D.L., & Evans, B.W. (2010). Abbreviations for names of rock–forming minerals. *American Mineralogist*, *95,* 185-187.

Ye Kyaw Thu, Enami, M., Kato, T., & Tsuboi, M. (2017). Granulite facies paragneisses from the middle segment of the Mogok metamorphic belt, central Myanmar. *Journal of Mineralogical and Petrological Sciences*, *112*, 1-19.

Ye Kyaw Thu, Maw Maw Win, Enami, M., & Tsuboi, M. (2016). Ti-rich biotite in spinel and quartz-bearing paragneiss and related rocks from the Mogok metamorphic belt, central Myanmar. *Journal of Mineralogical and Petrological Sciences*, *111*, 270-282.

Yonemura, K., Osanai, Y., Nakano, N., Adachi, T., Charusiri, P., & Tun Naing Zaw (2013). EPMA U-Th-Pb monazite dating of metamorphic rocks from the Mogok

Metamorphic Belt, central Myanmar. *Journal of Mineralogical and Petrological Sciences*, *108*, 184-188.

Yui, T.F., Zaw, K., & Wu, C.M. (2008). A preliminary stable isotope study on Mogok ruby, Myanmar. *Ore Geology Reviews*, *34,* 192-199.

Captions for Figures

FIGURE 1. Geological map of Myanmar and the adjacent regions showing major suture zones, faults, and terrane boundaries [modified from Figure 1 of Mitchell *et al*. (2007)].

FIGURE 2. Geological maps of (a) the middle segment of the Mogok metamorphic belt and the adjacent regions [part of Figure 2 of Mitchell *et al*. (2012)] and (b) detailed geological map of the sampling areas with sample localities [unpublished geological data by Myint Lwin Thein *et al*. (1990)].

FIGURE 3. Back-scattered electron (BSE) and X-ray mapping images showing textural characteristics of major constituent minerals of a marble (KST03) from the Mogok metamorphic belt. (a) and (b) Clinohumite and its inclusions and reaction relationship between clinohumite and calcite, (c) aggregates of phlogopite, pargasite, and secondary chlorite in matrix, (d) calcite grain with dolomite spherules included in a spinel, and (e) tremolite, diopside, and dolomite aggregate and (f) symplectitic aggregate of tremolite and dolomite between clinohumite and calcite. Numbers in (d) indicate mol% of magnesite component in calcite. Abbreviation for mineral: Tr-symp, symplectitic aggregate of tremolite and dolomite.

FIGURE 4. Back-scattered electron (BSE) and X-ray mapping images showing textural characteristics of major constituent minerals of marble from the Mogok metamorphic belt. (a) and (b) modes of occurrences of major phases of ZYK01, (c) calcite grains occurring as inclusions in spinel and the matrix phase of OZ01, (d) variations of Ca content of the matrix calcite showing exsolution textures of OZ01, (e) mode of occurrence of major phases of ACT01, and (f) variations of

Ca content of the matrix calcite, which locally contains exsolved dolomite of ACT01. Numbers in (f) indicate mol% of magnesite component in calcite.

FIGURE 5. Back-scattered electron (BSE) and X-ray mapping images showing textural characteristics of major constituent minerals of calc-silicate rock from the Mogok metamorphic belt. (a) Scapolite with sodic rim coexisting with diopside, calcite, K-feldspar, quartz, and titanite (OZ03), (b) Scapolite partly replaced by plagioclase (S-Pl), calcite, and small amounts of quartz (WBY01), (c) scapolite extensively replaced by clinozoisite (KB01), and (d) anorthite-rich plagioclase partly replaced by an aggregate of muscovite and quartz (WBY01). "Sodic Scp" indicates sodic scapolite rim around calcic scapolite. "P-Pl" and "S-Pl" imply primary ($An_{90–96}$) and secondary ($An_{75–85}$) plagioclase grains, respectively. Numbers indicate *EqAn* (a and c) and *An* (b and d) contents of representative analytical points.

FIGURE 6. Cumulative diagrams of (a) M_{Ti}/Si value and (b) F (wt %) of clinohumite in a marble from the Mogok metamorphic belt (KST03). M_{Ti} and "*n*" indicate total octahedral cations including Ti (Gaspar, 1992; Jones et al., 1969) and the ratio of the olivine layer to the brucite layer [nMg_2SiO_4•$Mg(F, OH)_2$], respectively.

FIGURE 7. Compositional range of phlogopite in marble from the Mogok metamorphic belt in (a) F (wt%) cumulative number, (b) K–Na–(Ba + Ca), (c) (Ba + Ca)–(K + Na), and (d) Si–(Ba + Ca) diagrams. □ denotes vacant-site.

FIGURE 8. Compositional range of scapolite and plagioclase in calc-silicate-rock from the Mogok metamorphic belt in *EqAn* [= (Al-3)/3 × 100] –X_{Cl} [= Cl/2 for total cations = 16 ≈ Cl/(Cl + CO_3)] diagram. Lines bracket the stoichiometric range of scapolite grains proposed by Evans, Shaw and Haughton (1969).

FIGURE 9. Compositional range of amphibole in marble and calc-silicate rock from the Mogok metamorphic belt in (a) Si–$^{[A]}$(Na + K) and (b) Si–X_F [= F/2 ≈ F/(F + Cl + OH)] diagrams.

FIGURE 10. Cumulative diagrams of magnesite mol% of calcite in marble from the Mogok metamorphic belt. Data showing magnesite content less than 2 mol% are omitted. Each integrated composition was estimated using dataset of a whole inclusion or core part of an exsolved matrix grain. Temperature conditions were estimated using a geothermometer proposed by Anovitz and Essene (1987).

FIGURE 11. Isobaric T–X_{CO2} diagrams in the calcite-excess system for the clinohumite-bearing marble of KST03 from the Mogok metamorphic belt at pressures of (a) 0.8 GPa and (b) 0.5 GPa. Fixed activities of clinohumite at temperatures of 800 °C and 600 °C were employed for calculations of the diagrams (a) and (b), respectively. The pressure dependence of the upper stability limit of X_{CO2} and temperature conditions of the reaction R3 Tr + 13Dol + H_2O = 2Chu + 15Cal + 11CO_2 is shown in (b) for the pressure range of 0.4–0.65 GPa. Labels R1–R5 correspond to reactions discussed in the text. H_2O and CO_2 components of reactions are omitted for convenience. Minerals other than quartz, which are in equilibrium with calcite, are shown in CaO–MgO–SiO_2 diagrams.

FIGURE 12. Isobaric T–X_{CO2} diagram in the quartz and calcite-excess system for the scapolite-bearing calc-silicate rock of WBY01 and OZ03 from the Mogok metamorphic belt showing stability relationship of scapolite and related phases at P = 0.8 GPa. Fixed activities of meionite and anorthite at temperatures of 800 °C, and that of grossular calculated as $(X_{Grs})^3$, assuming ideal solid solution

(where X_{Grs} implies molecular proportion of grossular), were employed for calculation of the diagrams. H_2O and CO_2 components of reactions are omitted for convenience. Labels R6–R8 correspond to those of the reactions discussed in the text.

FIGURE 13. Isobaric T–X_{CO2} diagrams for the scapolite-bearing calc-silicate rock of KB01 from the Mogok metamorphic belt showing stability relationships of scapolite and related phases (a) in the quartz and calcite-excess system at P = 0.8 GPa and (b) in the quartz-free and calcite-excess system under various pressure conditions between 0.4 and 0.8 GPa. Univariant lines of Wo = Qz + Cal at 0.5 and 0.8 GPa are superimposed on the diagram (b) to compare the stability conditions of Qz + Cal and Czo. Fixed activities of phases at temperatures of 800 °C and 750 °C were employed for calculations of the diagrams (a) and (b), respectively. H_2O and CO_2 components of reactions are omitted for convenience. Labels R6–R12 correspond to those of the reactions discussed in the text. Broken lines with arrow in (a) and (b) indicate shift trend of invariant points [Mei, Wo] and [Grs, Wo], respectively.

FIGURE 14. Schematic diagram showing evolution of fluid compositions of marble, calc-silicate rock, and paragneiss from the middle segment of the Mogok metamorphic belt in Myanmar. The stabilities of aluminum silicates are from Pattison (2001). References for *P-T* estimations of paragneiss are Y16, Ye Kyaw Thu *et al*. (2016); Y17, Ye Kyaw Thu *et al*. (2017).

Caption for Tables

Table 1. Mineral assemblages in marble and calc-silicate rock from the Onzon-Thabeikkyin region of the Mogok metamorphic belt, Myanmar.
+, prograde phase in matrix; i, inclusion phase in primary phase; ei, exsolved phase in calcite inclusion; em, exsolved phase in matrix calcite; r, retrograde phase; ce, coalescence phase of exsolved dolomite.
Note: 1) In the matrix calcite, exsolution texture is observed only as narrow marginal zone (100–200 μm in width) in some grains, 2) Calcite inclusion in diopside do not show exsolution texture.

Table 2. Representative chemical compositions of major constituent minerals of marble from the Onzon-Thabeikkyin region of the Mogok metamorphic belt, Myanmar.
* Total iron as FeO.
** Calculated values.
Abbreviations for texture: Pgp, prograde phase; Rgp, retrograde phase; Symp, retrograde symplectitic phase.

Table 3. Representative chemical compositions of major constituent minerals of calc-silicate rock from the Onzon-Thabeikkyin region of the Mogok metamorphic belt, Myanmar.
* Total iron as FeO.
** Total iron as Fe_2O_3.
† Total cations as 16.
§ Calculated value (see text).
Abbreviations for texture: Pgp, prograde phase; Rgp, retrograde phase.

Table 4. Chemical compositions of minerals employed for the calculations of T-X_{CO2} diagrams.

* Anorthite content was estimated assuming that An/EqAn = 1.2 considering the pair of prograde scapolite and plagioclase in WBY01.

** X_{Mg} value was assumed to be same with that of diopside.

Abbreviations for texture: Pgp, prograde phase; Rgp, retrograde phase.

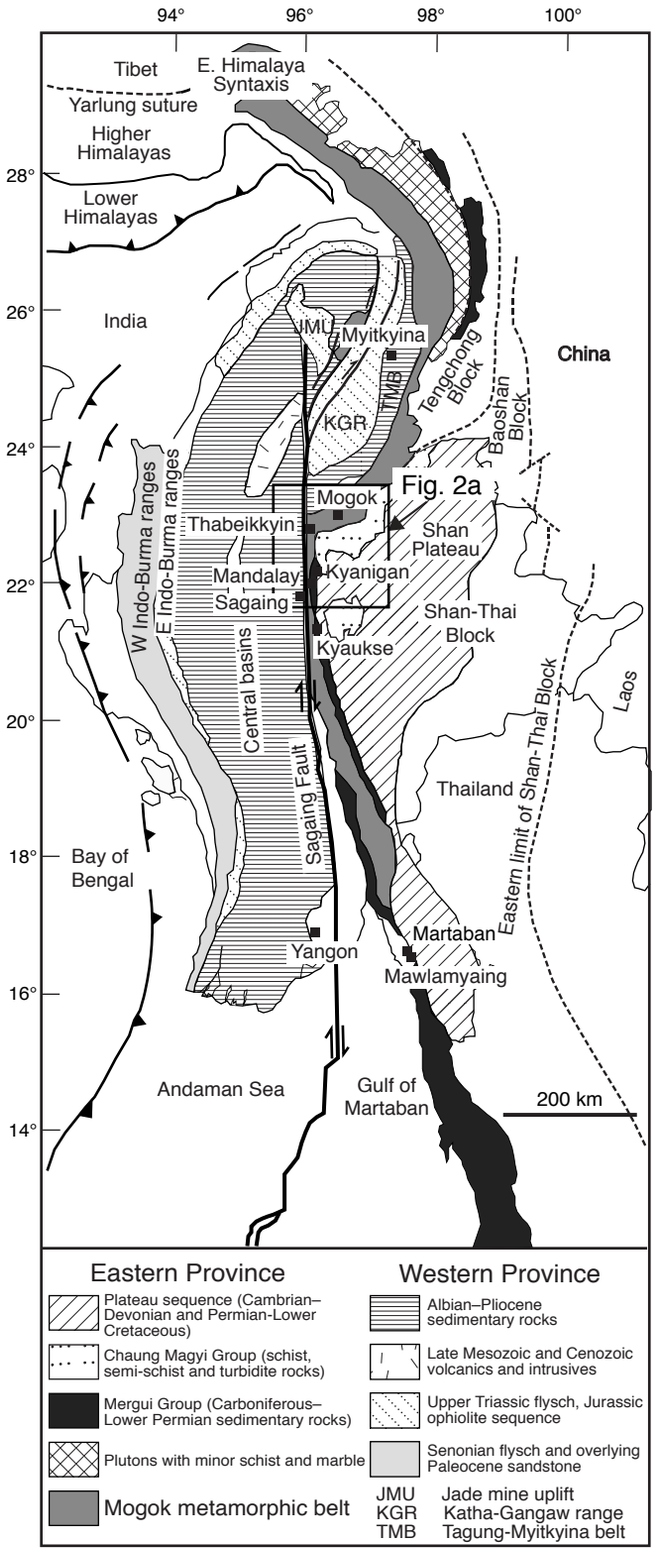

FIGURE 1. Geological map of Myanmar and the adjacent regions showing major suture zones, faults, and terrane boundaries [modified from Figure 1 of Mitchell et al. (2007)].

FIGURE 01 (Ye Kyaw Thu and Enami)

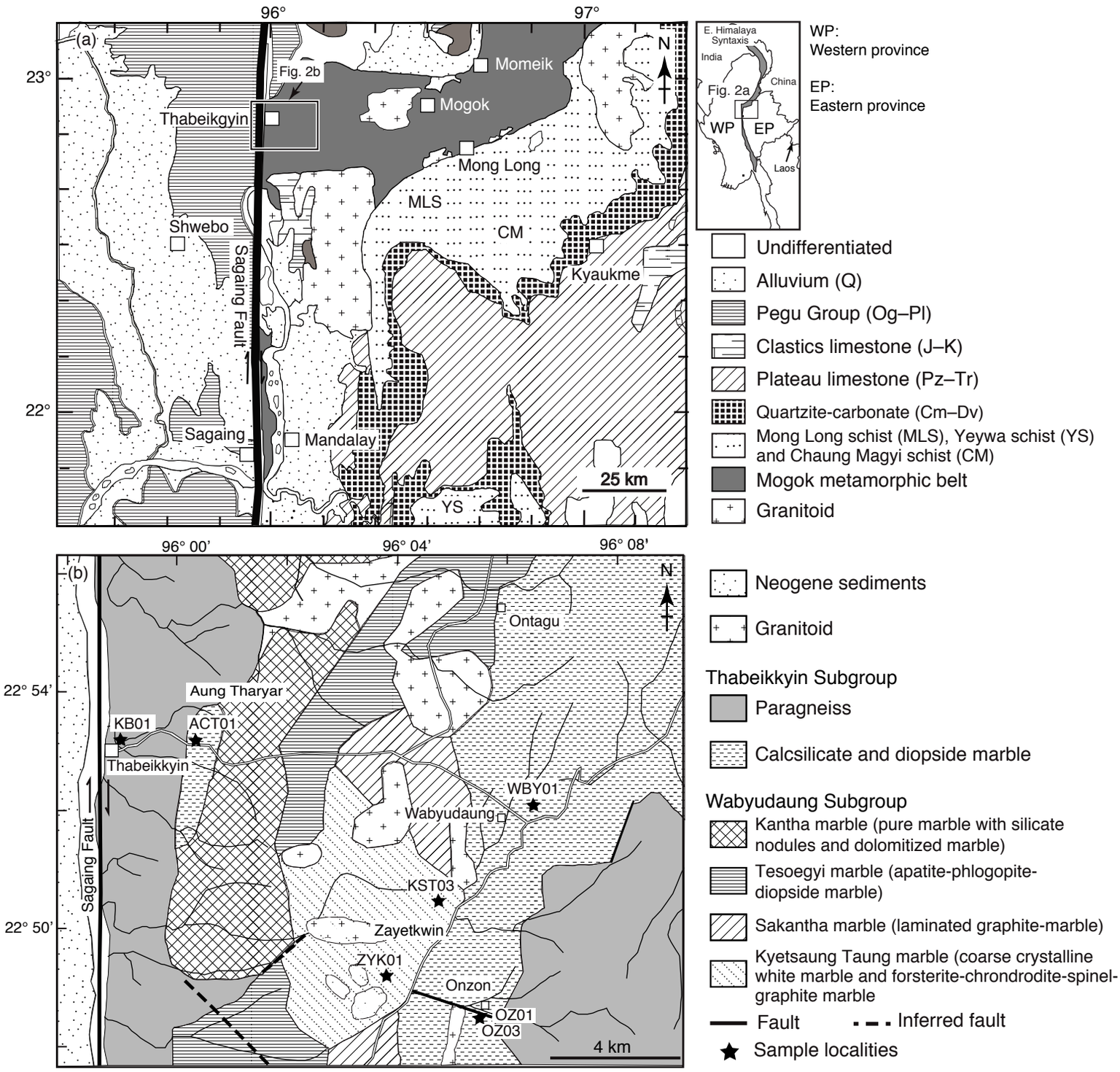

FIGURE 2. Geological maps of (a) the middle segment of the Mogok metamorphic belt and the adjacent regions [part of Figure 2 of Mitchell et al. (2012)] and (b) detailed geological map of the sampling areas with sample localities [unpublished geological data by Myint Lwin Thein et al. (1990)].

FIGURE 02 (Ye Kyaw Thu and Enami)

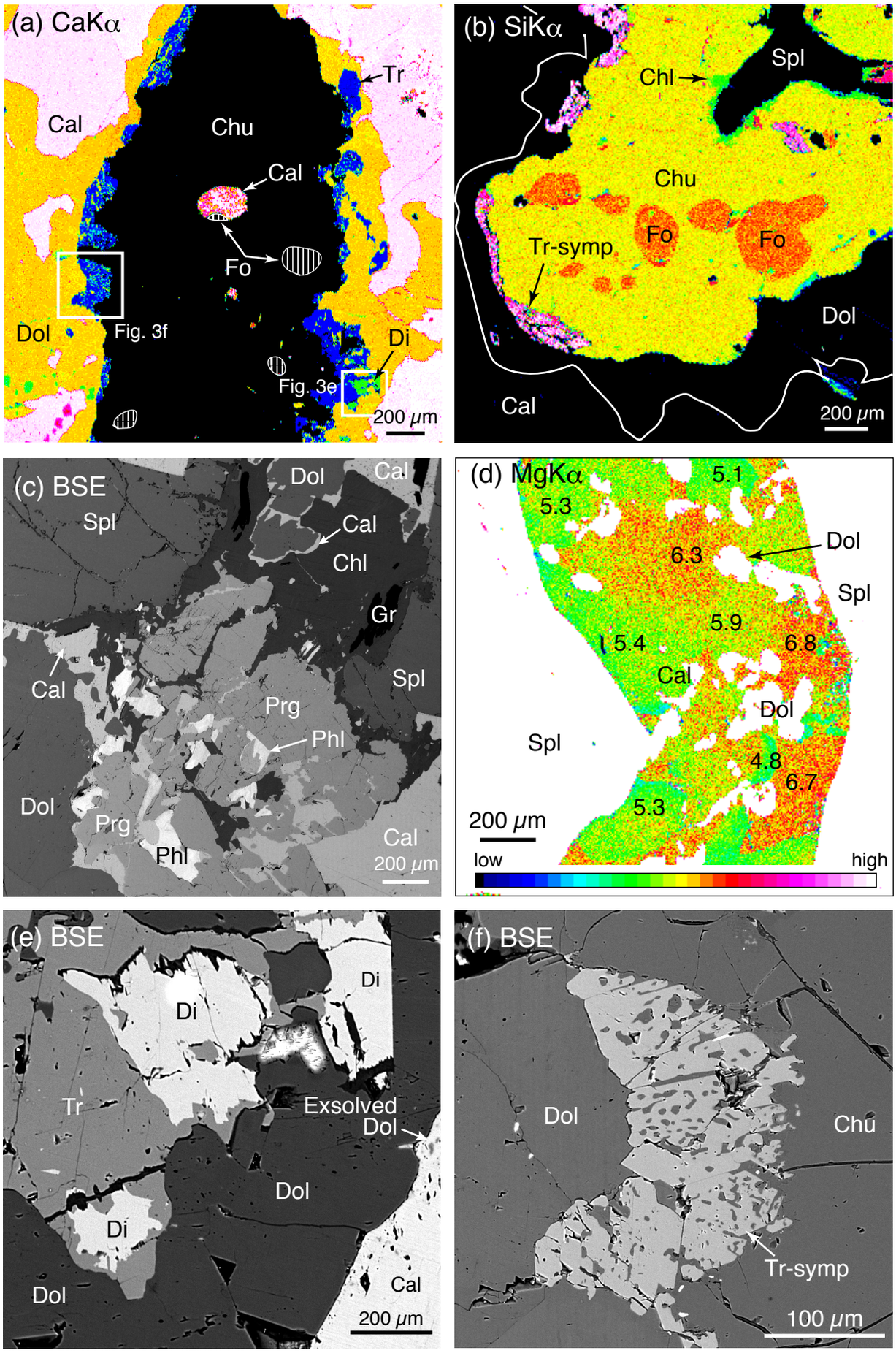

FIGURE 3. Back-scattered electron (BSE) and X-ray mapping images showing textural characteristics of major constituent minerals of a marble (KST03) from the Mogok metamorphic belt. (a) and (b) Clinohumite and its inclusions and reaction relationship between clinohumite and calcite, (c) aggregates of phlogopite, pargasite, and secondary chlorite in matrix, (d) calcite grain with dolomite spherules included in a spinel, and (e) tremolite, diopside, and dolomite aggregate and (f) symplectitic aggregate of tremolite and dolomite between clinohumite and calcite. Numbers in (d) indicate mol% of magnesite component in calcite. Abbreviation for mineral: Tr-symp, symplectitic aggregate of tremolite and dolomite.

FIGURE 03 (Ye Kyaw Thu and Enami)

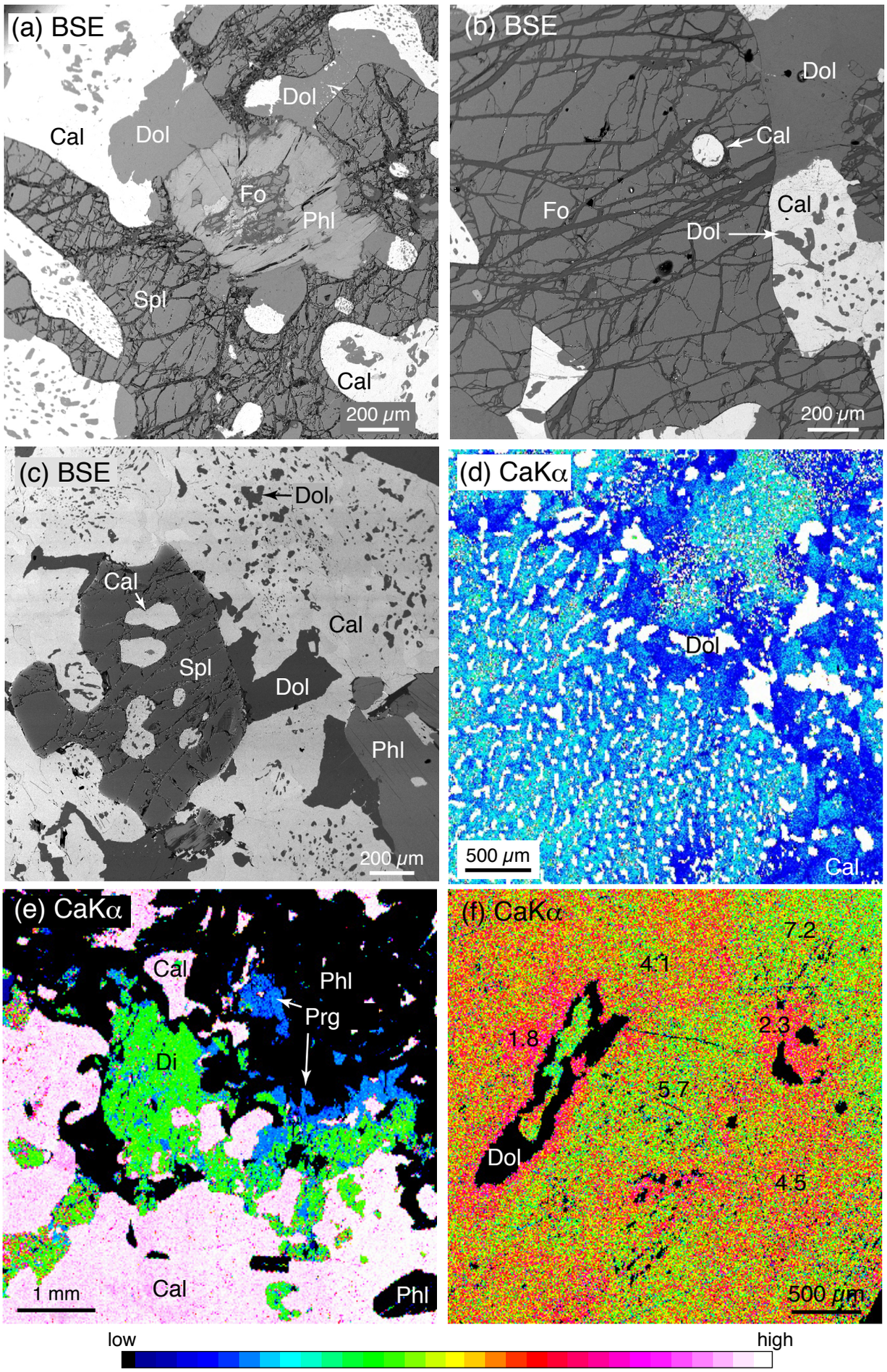

FIGURE 4. Back-scattered electron (BSE) and X-ray mapping images showing textural characteristics of major constituent minerals of marble from the Mogok metamorphic belt. (a) and (b) modes of occurrences of major phases of ZYK01, (c) calcite grains occurring as inclusions in spinel and the matrix phase of OZ01, (d) variations of Ca content of the matrix calcite showing exsolution textures of OZ01, (e) mode of occurrence of major phases of ACT01, and (f) variations of Ca content of the matrix calcite, which locally contains exsolved dolomite of ACT01. Numbers in (f) indicate mol% of magnesite component in calcite.

FIGURE 04 (Ye Kyaw Thu and Enami)

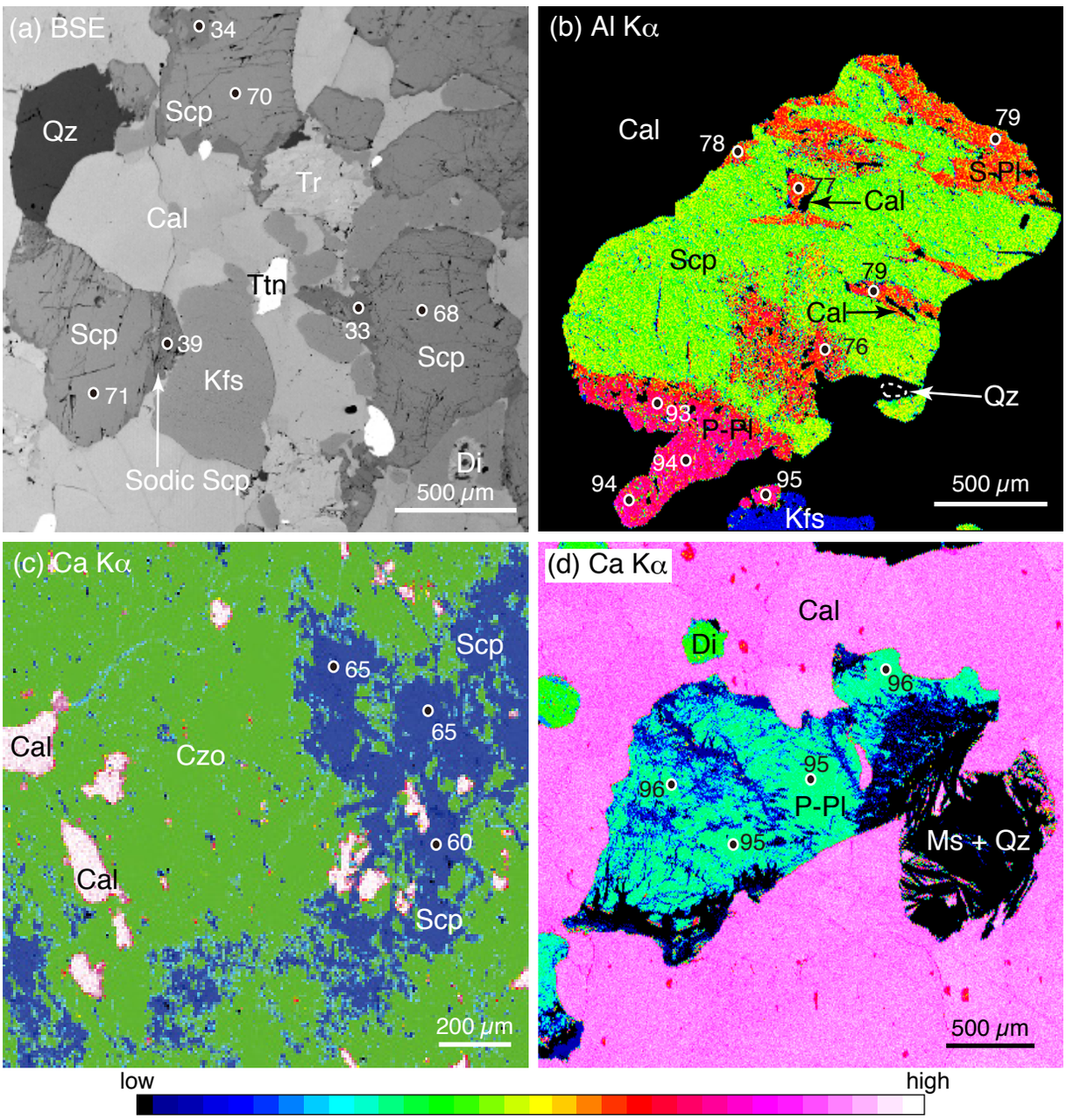

FIGURE 5. Back-scattered electron (BSE) and X-ray mapping images showing textural characteristics of major constituent minerals of calc-silicate rock from the Mogok metamorphic belt. (a) Scapolite with sodic rim coexisting with diopside, calcite, K-feldspar, quartz, and titanite (OZ03), (b) Scapolite partly replaced by plagioclase (S-Pl), calcite, and small amounts of quartz (WBY01), (c) scapolite extensively replaced by clinozoisite (KB01), and (d) anorthite-rich plagioclase partly replaced by an aggregate of muscovite and quartz (WBY01). "Sodic Scp" indicates sodic scapolite rim around calcic scapolite. "P-Pl" and "S-Pl" imply primary (An90–96) and secondary (An75–85) plagioclase grains, respectively. Numbers indicate EqAn (a and c) and An (b and d) contents of representative analytical points.

FIGURE 05 (Ye Kyaw Thu and Enami)

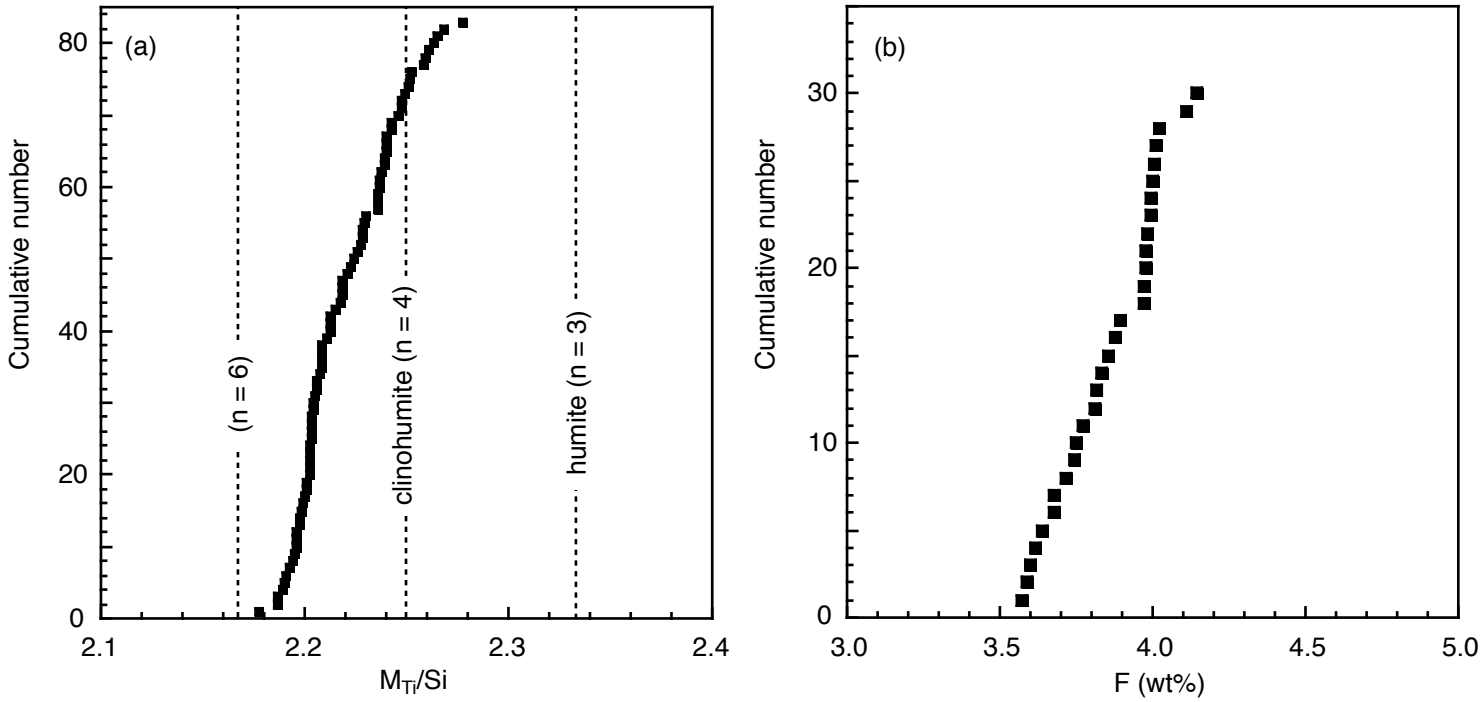

FIGURE 6. Cumulative diagrams of (a) MTi/Si value and (b) F (wt %) of clinohumite in a marble from the Mogok metamorphic belt (KST03). MTi and "n" indicate total octahedral cations including Ti (Gaspar, 1992; Jones et al., 1969) and the ratio of the olivine layer to the brucite layer [$nMg_2SiO_4 \cdot Mg(F, OH)_2$], respectively.

FIGURE 06 (Ye Kyaw Thu and Enami)

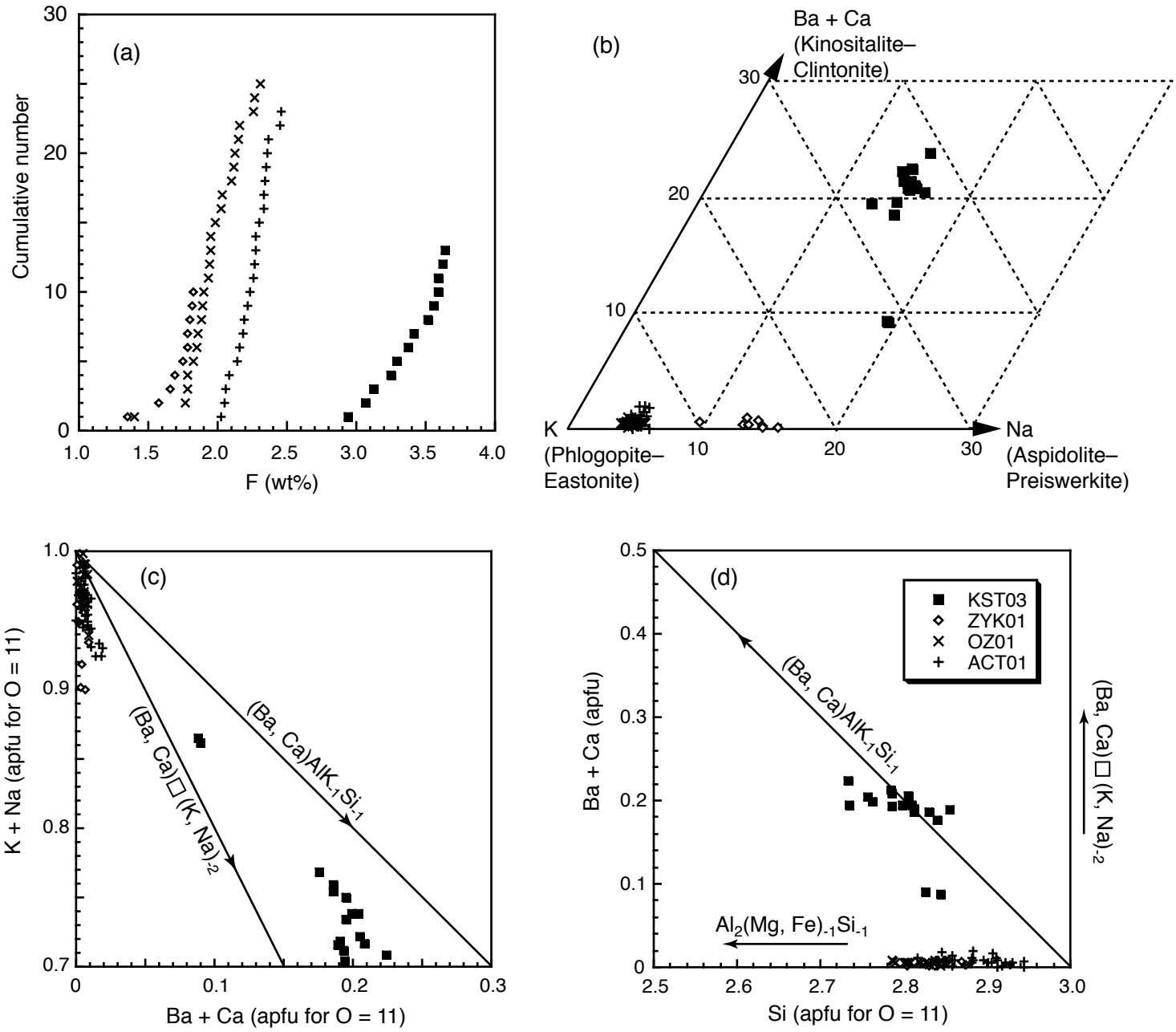

FIGURE 7. Compositional range of phlogopite in marbles from the Mogok metamorphic belt in (a) F (wt%) cumulative number, (b) K–Na–(Ba + Ca), (c) (Ba + Ca)–(K + Na), and (d) Si–(Ba + Ca) diagrams. □ denotes vacant-site.

FIGURE 07 (Ye Kyaw Thu and Enami)

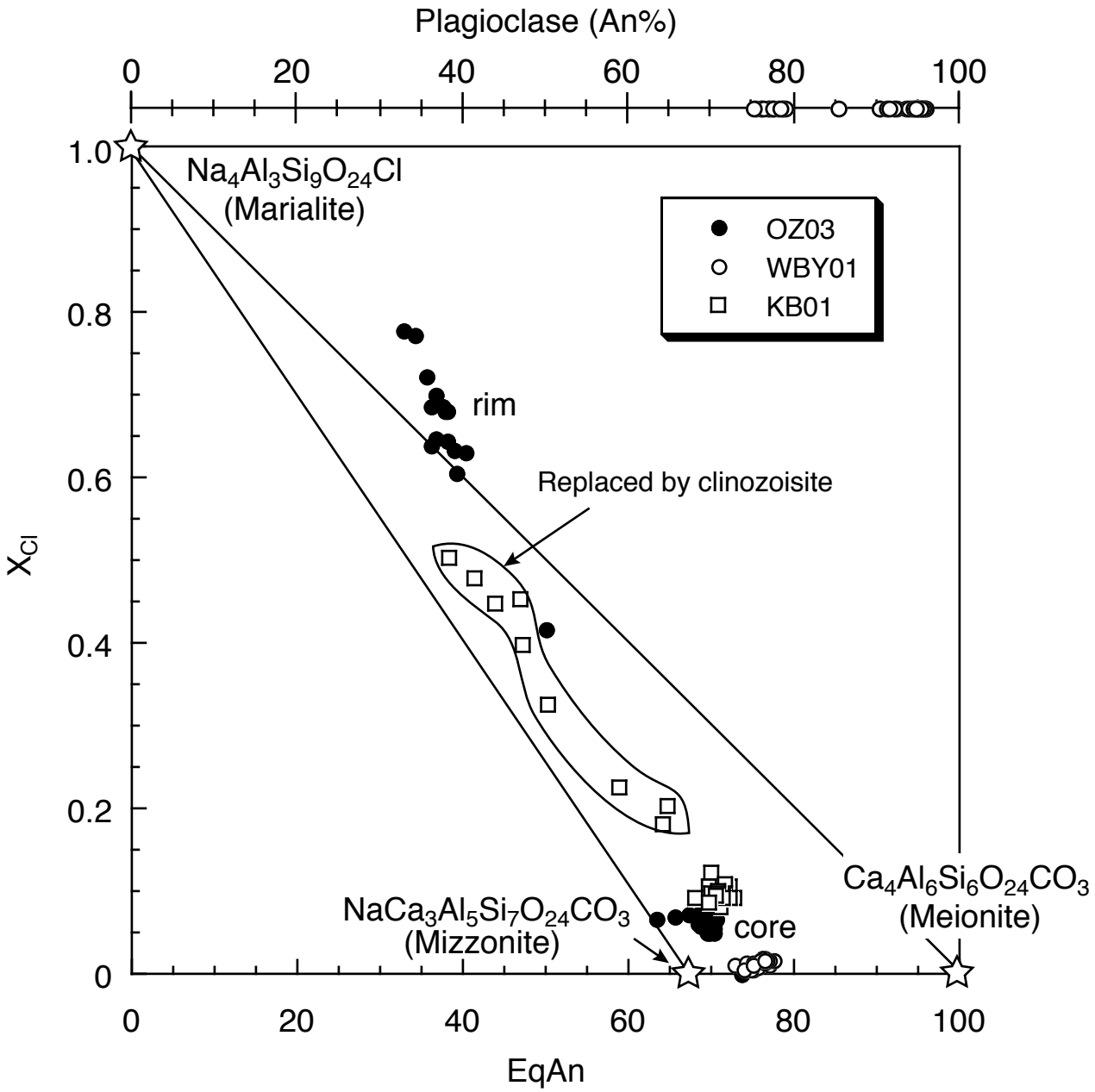

FIGURE 8. Compositional range of scapolite and plagioclase in calc-silicate-rock from the Mogok metamorphic belt in EqAn [= (Al-3)/3 X 100] –XCl [= Cl/2 for total cations = 16 ≈ Cl/(Cl + CO3)] diagram. Lines bracket the stoichiometric range of scapolite grains proposed by Evans, Shaw & Haughton (1969).

FIGURE 08 (Ye Kyaw Thu and Enami)

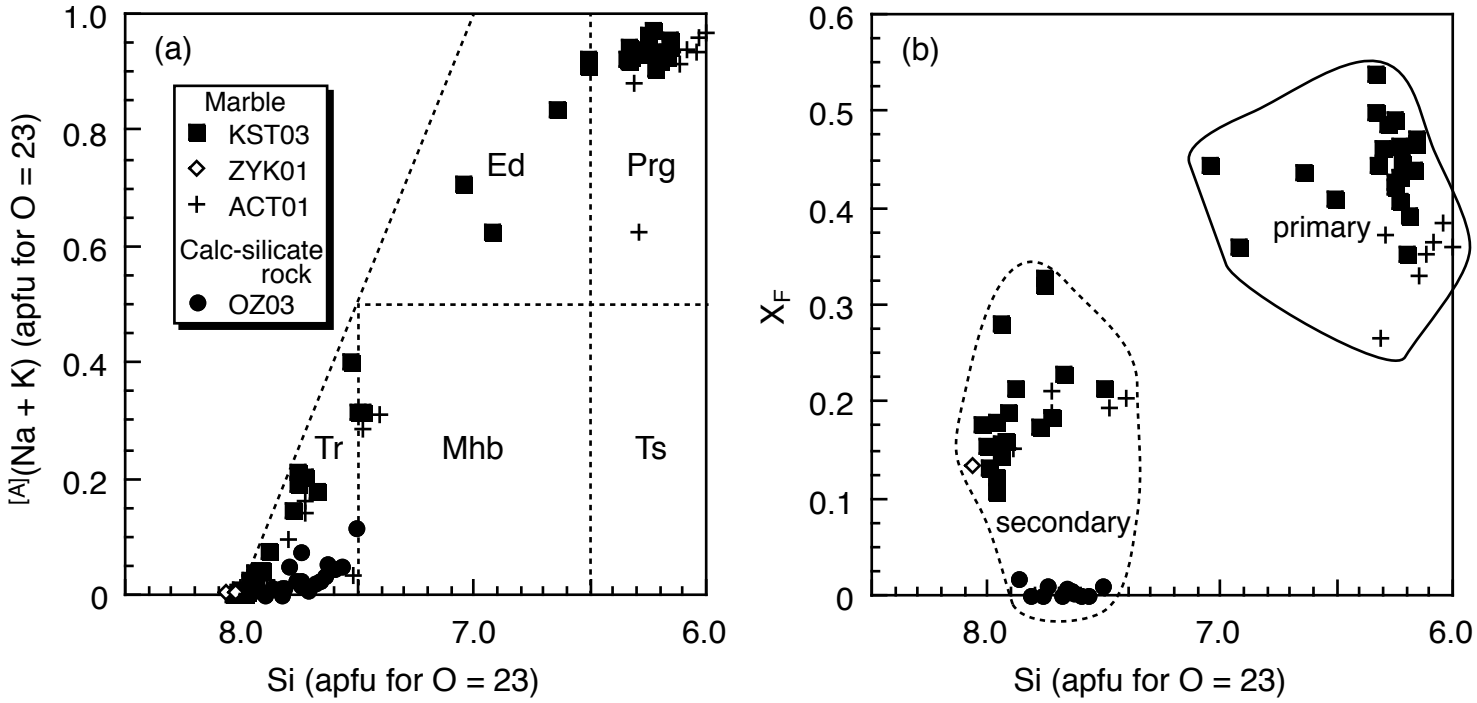

FIGURE 9. Compositional range of amphibole in marbles and calc-silicate rock from the Mogok metamorphic belt in (a) Si–$^{[A]}$(Na + K) and (b) Si–X_F [= F/2 ≈ F/(F + Cl + OH)] diagrams.

FIGURE 09 (Ye Kyaw Thu and Enami)

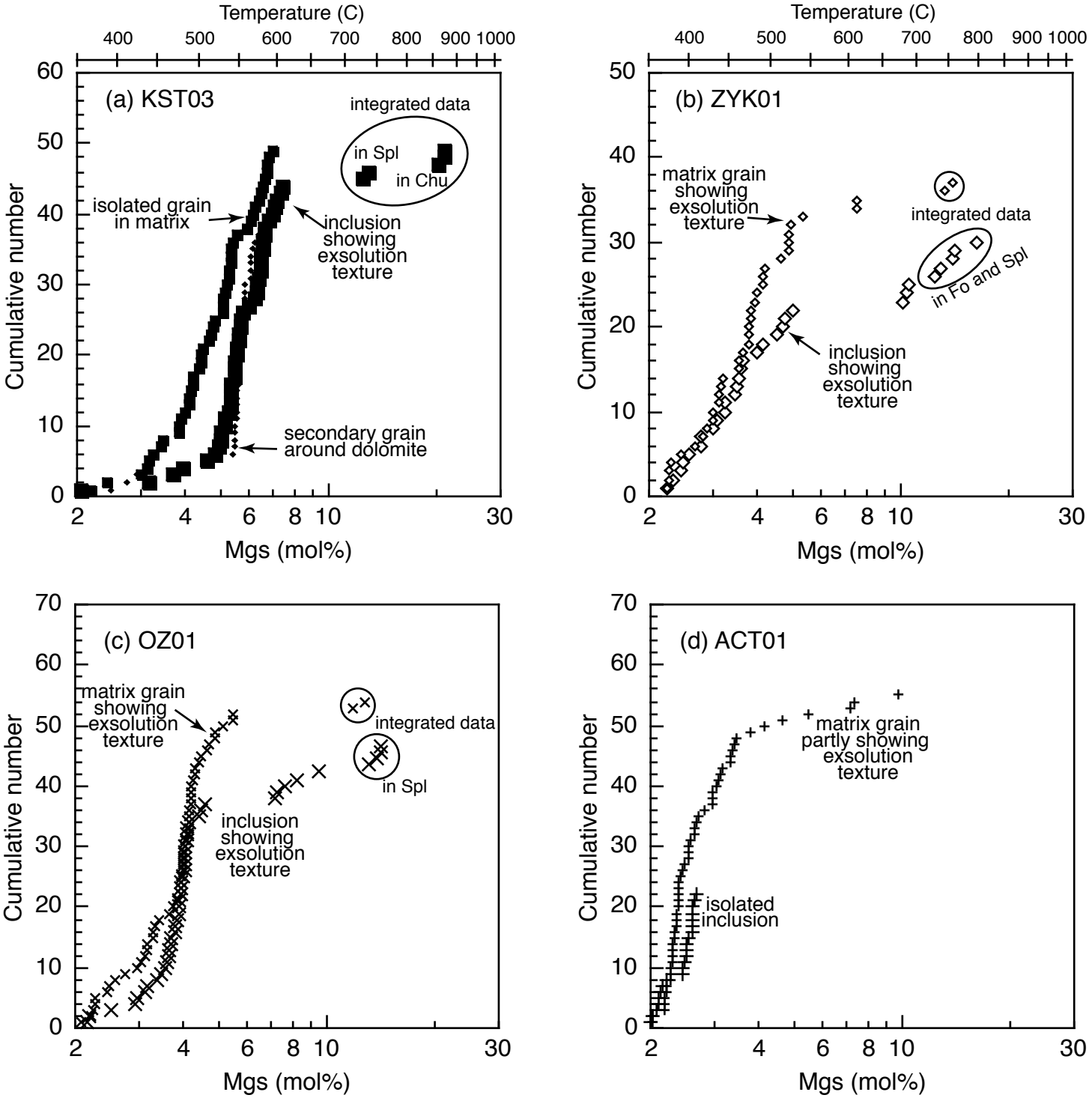

FIGURE 10. Cumulative diagrams of magnesite mol% of calcite in marble from the Mogok metamorphic belt. Data showing magnesite content less than 2 mol% are omitted. Each integrated composition was estimated using dataset of a whole inclusion or core part of an exsolved matrix grain. Temperature conditions were estimated using a geothermometer proposed by Anovitz and Essene (1987).

FIGURE 10 (Ye Kyaw Thu and Enami)

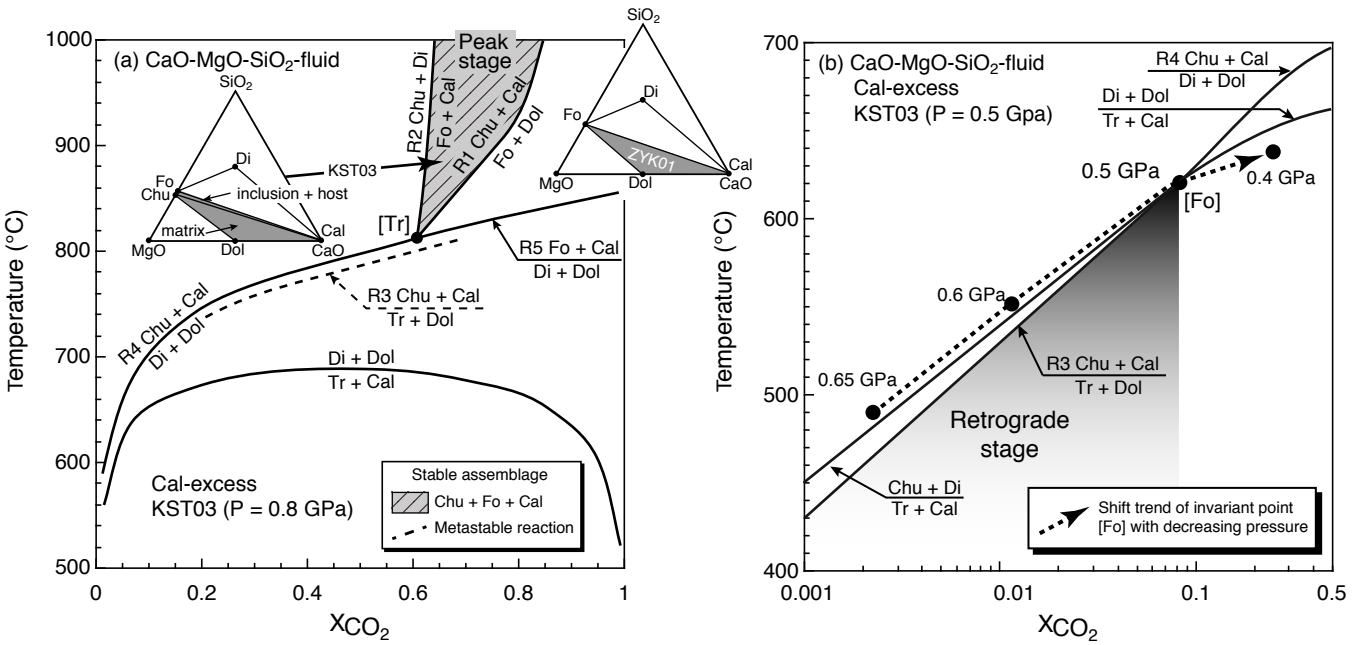

FIGURE 11. Isobaric T–XCO2 diagrams in the calcite-excess system for the clinohumite-bearing marble of KST03 from the Mogok metamorphic belt at pressures of (a) 0.8 GPa and (b) 0.5 GPa. Fixed activities of clinohumite at temperatures of 800 °C and 600 °C were employed for calculations of the diagrams (a) and (b), respectively. The pressure dependence of the upper stability limit of XCO2 and temperature conditions of the reaction R3 Tr + 13Dol + H2O = 2Chu + 15Cal + 11CO2 is shown in (b) for the pressure range of 0.4–0.65 GPa. Labels R1–R5 correspond to reactions discussed in the text. H2O and CO2 components of reactions are omitted for convenience. Minerals other than quartz, which are in equilibrium with calcite, are shown in CaO–MgO–SiO2 diagrams.

FIGURE 11 (Ye Kyaw Thu and Enami)

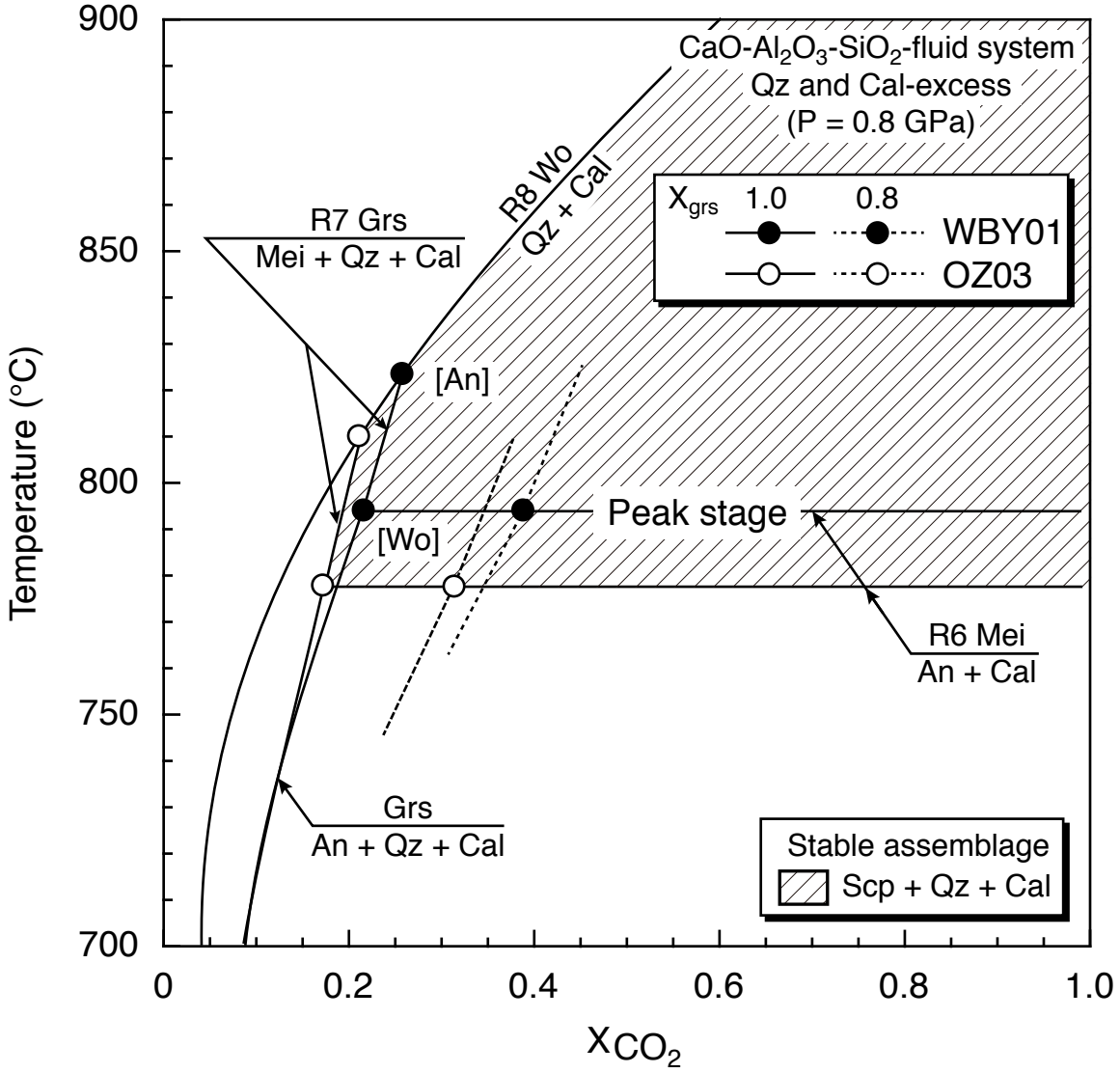

FIGURE 12. Isobaric T–XCO2 diagram in the quartz and calcite-excess system for the scapolite-bearing calc-silicate rock of WBY01 and OZ03 from the Mogok metamorphic belt showing stability relationship of scapolite and related phases at P = 0.8 GPa. Fixed activities of meionite and anorthite at temperatures of 800 °C, and that of grossular calculated as (XGrs)3,· assuming ideal solid solution (where XGrs implies molecular proportion of grossular), were employed for calculation of the diagrams. H2O and CO2 components of reactions are omitted for convenience. Labels R6–R8 correspond to those of the reactions discussed in the text.

FIGURE 12 (Ye Kyaw Thu and Enami)

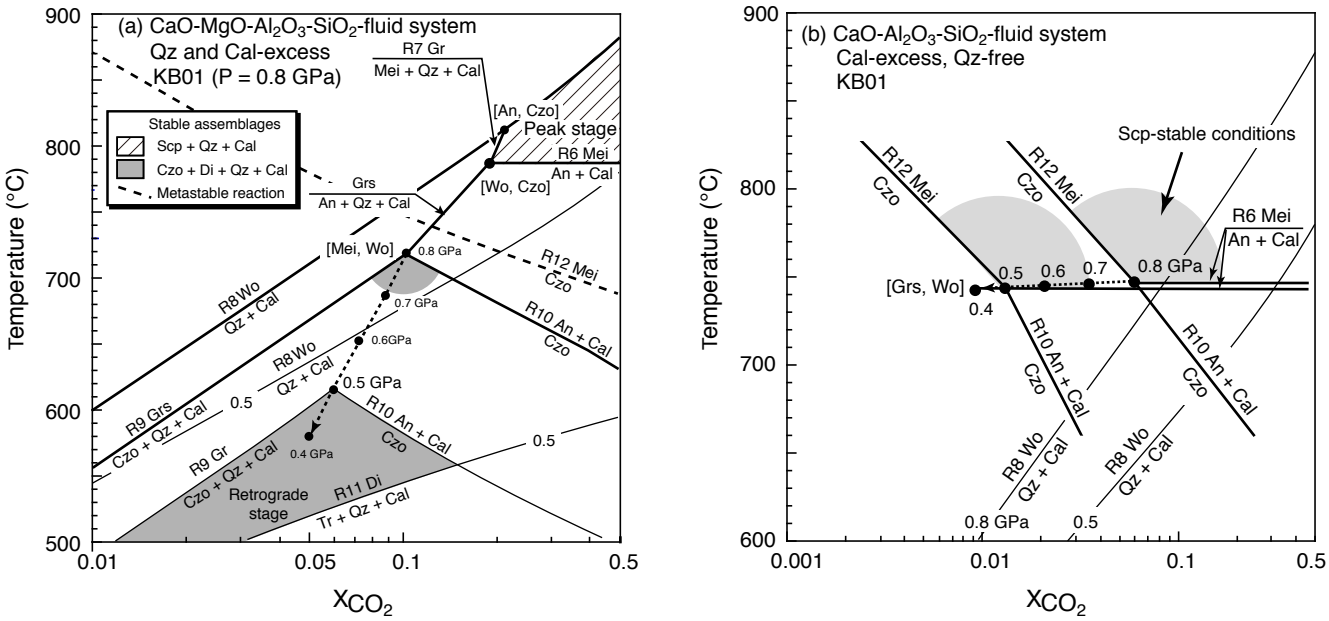

FIGURE 13. Isobaric T–XCO2 diagrams for the scapolite-bearing calc-silicate rock of KB01 from the Mogok metamorphic belt showing stability relationships of scapolite and related phases (a) in the quartz and calcite-excess system at P = 0.8 GPa and (b) in the quartz-free and calcite-excess system under various pressure conditions between 0.4 and 0.8 GPa. Univariant lines of Wo = Qz + Cal at 0.5 and 0.8 GPa are superimposed on the diagram (b) to compare the stability conditions of Qz + Cal and Czo. Fixed activities of phases at temperatures of 800 °C and 750 °C were employed for calculations of the diagrams (a) and (b), respectively. H_2O and CO_2 components of reactions are omitted for convenience. Labels R6–R12 correspond to those of the reactions discussed in the text. Broken lines with arrow in (a) and (b) indicate shift trend of invariant points [Mei, Wo] and [Grs, Wo], respectively.

FUGURE 13 (Ye Kyaw Thu and Enami)

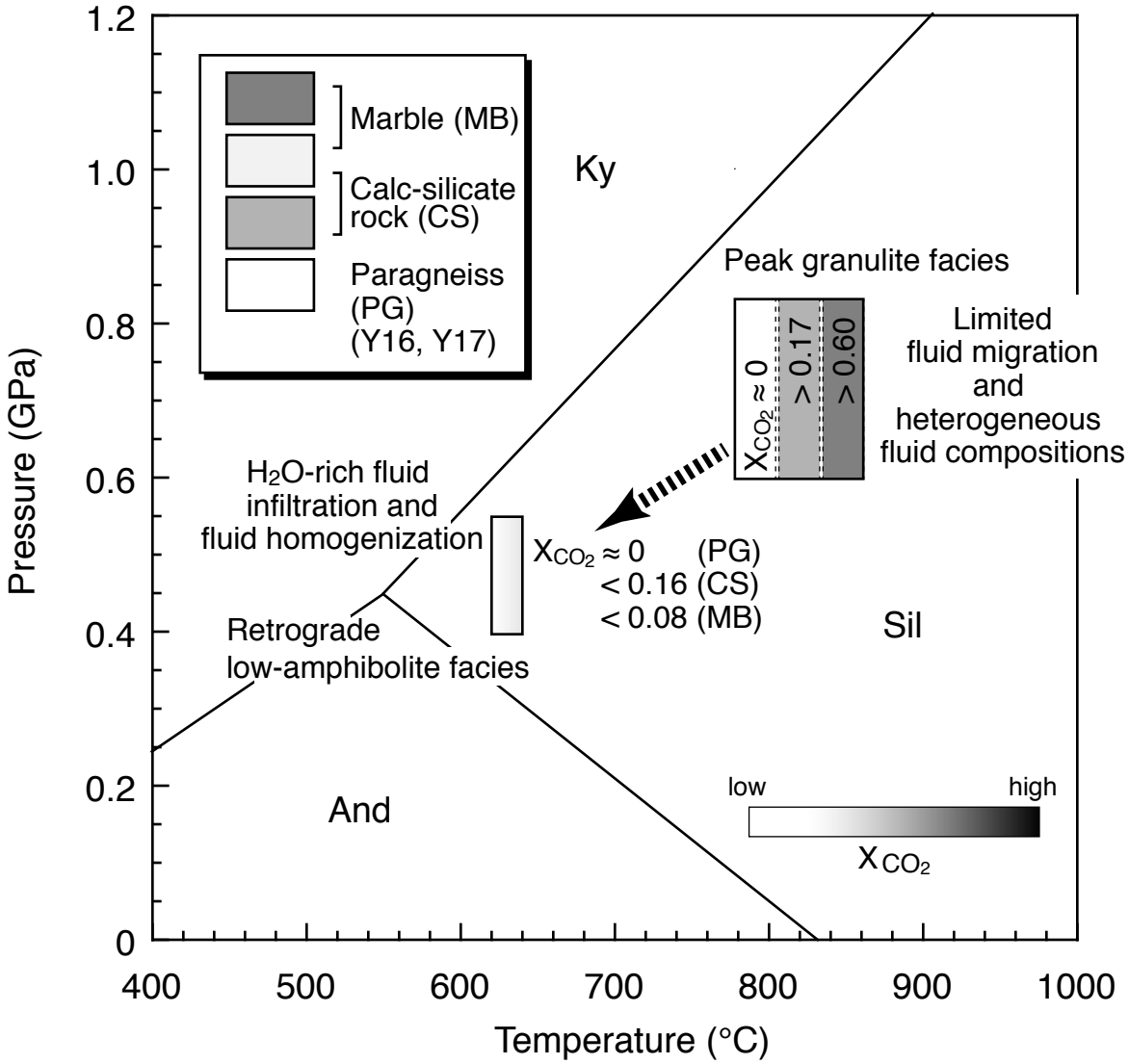

FIGURE 14. Schematic diagram showing evolution of fluid compositions of marble, calc-silicate rock, and paragneiss from the middle segment of the Mogok metamorphic belt in Myanmar. The stabilities of aluminum silicates are from Pattison (2001). References for P-T estimations of paragneiss are Y16, Ye Kyaw Thu et al. (2016); Y17, Ye Kyaw Thu et al. (2017).

FIGURE 14 Ye Kyaw Thu and Enami)

Table 1. Mineral assemblages in dolomitic marbl and calc-silicate rock from the Onzon-Thabeikkyin region of the Mogok metamorphic belt, Myanmar.

Sample	Cal	Dol	Chu	Spl	Fo	Di	Phl	Prg/Ed	Tr	Scp	Pl	Qz	Czo	Ttn	Others	Note
Marble																
KST03	+, i	is, ei	+	+, i	i	r	+	+	r						Gr/Chl	1)
ZYK01	+, i	is, ei, em		+	+		+		r						Srp	
OZ01	+, i	ce, ei, em		+			+								Chl	
ACT01	+, i	em				+	+	+	r						Gr	2)
Calc-silicate rock																
OZ03	+, i					+			r	+, i, r		+		+, i	Kfs	
WBY01	+, r					+				+	+, r	+		+	Kfs/Ms	
KB01	+					+				+, r		+	r	+, i	Kfs	

+, prograde phase in matrix; i, inclusion phase in primary phase; is, isolated phase in matrix; ei, exsolved phase in calcite inclusion in primary phases; r, retrograde phase; em, exslved phase in matrix calcite; ce, coalescence phase of exsolved dolomite.

Note: 1) In the matrix calcite, exsolution texture is observed only as narroue marginal zone (100–200 μm in width) in some grains, 2) Calcite incluion in dipside do not show exsolution texture.

Table 2. Representative chemical compositions of major constituent minerals of marble from the Onzon-Thabeikkyin region of the Mogok metamorphic belt, Myanmar.

Sample	KST03								
Mineral	Chu	Chu	Fo	Phl	Phl	Spl	Prg	Tr	Di
Note	Pgp	Pgp	Pgp	Pgp	Pgp	Pgp	Pgp	symp	symp
wt%									
SiO_2	38.27	38.44	43.40	38.03	38.90	0.00	45.06	59.34	55.62
TiO_2	0.06	0.04	0.00	0.30	0.28	0.03	0.14	0.04	0.01
Al_2O_3	0.01	0.00	0.01	16.29	15.23	70.19	14.24	0.20	0.28
Cr_2O_3	0.00	0.00	0.00	0.00	0.00	0.01	0.07	0.02	0.00
V_2O_3						1.21			
FeO*	0.25	0.22	0.40	0.02	0.03	0.40	0.10	0.04	0.09
MnO	0.00	0.00	0.00	0.00	0.02	0.03	0.00	0.00	0.00
MgO	57.36	58.16	57.57	26.63	27.10	28.00	20.66	24.54	18.66
NiO			0.01						
ZnO						0.39			
BaO				7.86	7.40	0.00			
CaO	0.02	0.02	0.01	0.05	0.05	0.00	12.94	13.80	25.34
Na_2O	0.00	0.00	0.00	1.02	0.98	0.00	3.35	0.09	0.03
K_2O	0.00	0.00	0.00	6.18	6.43		0.22	0.05	0.01
F	4.14	3.62		3.37	3.63		2.47	0.73	
Cl	0.00	0.01		0.06	0.06		0.06	0.01	
O=F, Cl	1.74	1.53		1.43	1.54		1.05	0.31	
Total	98.37	98.98	101.40	98.38	98.57	100.26	98.26	98.55	100.04
Formula									
O	17	17	4	11	11	4	23	23	6
Si	4.01	3.99	1.00	2.73	2.79	0.00	6.33	8.00	2.00
Ti	0.01	0.00	0.00	0.02	0.02	0.00	0.02	0.00	0.00
Al	0.00	0.00	0.00	1.38	1.29	1.97	2.36	0.03	0.01
Cr	0.00	0.00	0.00	0.00	0.00	0.00	0.01	0.00	0.00
V						0.02			
Fe^{3+**}						0.01	0.01	0.00	
Fe^{2+**}	0.02	0.02	0.01	0.00	0.00	0.00	0.01	0.01	0.00
Mn	0.00	0.00	0.00	0.00	0.00	0.00	0.00	0.00	0.00
Mg	8.95	8.99	1.98	2.85	2.89	0.99	4.33	4.93	1.00
Ni			0.00						0.00
Zn						0.01			0.00
Ba	0.00	0.00		0.22	0.21	0.00			0.00
Ca	0.00	0.00	0.00	0.00	0.00	0.00	1.95	1.99	0.98
Na	0.00	0.00	0.00	0.14	0.14	0.00	0.91	0.02	0.00
K	0.00	0.00	0.00	0.57	0.59		0.04	0.01	0.00
Total	12.99	13.01	3.00	7.92	7.92	3.00	15.95	15.00	3.99
F	1.37	1.19		0.77	0.82		1.10	0.31	
Cl	0.00	0.00		0.01	0.01		0.01	0.00	

* Total iron as FeO.

** Calculated values.

Abbreviations for texture: Pgp, prograde phase; Rgp, retrograde phase; Symp, retrograde symplectitic phase.

Table 2 (continued).

Sample	ZYK01				OZ01		ACT01			
Mineral	Fo	Phl	Spl	Tr	Phl	Spl	Phl	Di	Prg	Tr
Note	Pgp	Pgp	Pgp	Rgp	Pgp	Pgp	Pgp	Pgp	Pgp	Rgp
wt%										
SiO_2	42.50	41.70	0.03	59.03	40.28	0.01	41.80	51.43	42.45	58.61
TiO_2	0.00	0.16	0.06	0.04	0.86	0.04	0.20	0.35	0.22	0.05
Al_2O_3	0.00	16.59	71.17	0.09	16.72	70.01	14.89	5.18	17.41	1.54
Cr_2O_3	0.02	0.00	0.00	0.01	0.00	0.00	0.00	0.01	0.06	0.01
V_2O_3			0.10			0.05				
FeO*	0.69	0.14	0.77	0.14	0.41	1.91	1.29	2.02	2.05	1.73
MnO	0.02	0.01	0.02	0.01	0.00	0.01	0.01	0.04	0.01	0.00
MgO	56.33	26.75	26.99	24.90	25.84	25.53	26.51	15.42	18.23	22.94
NiO	0.04									
ZnO	0.00	0.00	0.16		0.02	1.96	0.17	0.00		
BaO		0.09			0.16		0.19			
CaO	0.00	0.01	0.00	13.92	0.04	0.00	0.05	24.82	13.06	13.38
Na_2O	0.00	0.91	0.00	0.08	0.33	0.00	0.32	0.34	2.30	0.29
K_2O	0.00	8.88	0.00	0.03	10.26	0.00	10.13	0.00	1.99	0.08
F		1.68		0.62	2.12		2.45		1.63	0.71
Cl		0.03		0.02	0.02		0.06		0.06	0.00
O=F, Cl		0.71		0.27	0.90		1.05		0.70	0.30
Total	99.60	96.24	99.30	98.62	96.16	99.52	97.02	99.61	98.77	99.04
Formula										
O	4	11	4	23	11	4	11	6	23	23
Si	1.00	2.88	0.00	7.96	2.82	0.00	2.91	1.88	6.00	7.91
Ti	0.00	0.01	0.00	0.00	0.05	0.00	0.01	0.01	0.02	0.01
Al	0.00	1.35	2.01	0.01	1.38	2.00	1.22	0.22	2.90	0.25
Cr	0.00	0.00	0.00	0.00	0.00	0.00	0.00	0.00	0.01	0.00
V			0.00			0.00				
Fe^{3+**}			0.00	0.01		0.00			0.09	0.00
Fe^{2+**}	0.01	0.01	0.02	0.00	0.02	0.04	0.08	0.06	0.16	0.20
Mn	0.00	0.00	0.00	0.00	0.00	0.00	0.00	0.00	0.00	0.00
Mg	1.98	2.75	0.96	5.00	2.69	0.92	2.75	0.84	3.84	4.62
Ni	0.00									
Zn	0.00	0.00	0.00		0.00	0.04	0.01	0.00		
Ba		0.00			0.00		0.01			
Ca	0.00	0.00	0.00	2.01	0.00	0.00	0.00	0.97	1.98	1.94
Na	0.00	0.12	0.00	0.02	0.05	0.00	0.04	0.02	0.63	0.08
K	0.00	0.78	0.00	0.01	0.92	0.00	0.90	0.00	0.36	0.01
Total	3.00	7.90	2.99	15.04	7.93	3.00	7.94	4.01	15.98	15.00
F		0.37		0.26	0.47		0.54		0.73	0.30
Cl		0.00		0.00	0.00		0.01		0.01	0.00

Table 3. Representative chemical compositions of major constituent minerals of calc-silicate rock from the Onzon-Thabeikkyin region of the Mogok metamorphic belt, Myanmar.

Sample	OZ03				WBY01					KB01		
Mineral	Scp	Scp	Di	Tr	Scp	Pl	Pl	Di	Ms	Scp	Scp	Czo
Note	core (Pgp)	mantle (Rgp)	Pgp	Rgp	Pgp	Pgp	Rgp	Pgp	Rgp	Pgp	Rgp	Rgp
wt%												
SiO_2	45.21	54.62	52.62	54.64	43.13	44.27	49.55	52.66	46.75	44.17	51.62	38.74
TiO_2	0.01	0.00	0.16	0.17	0.03	0.00	0.00	0.07	0.02	0.00	0.02	0.05
Al_2O_3	27.98	23.83	1.81	2.10	29.15	35.46	32.50	0.94	33.10	28.36	25.5	27.76
Cr_2O_3	0.00	0.00	0.06	0.06	0.03	0.00	0.03	0.03	0.00	0.00	0.00	0.02
FeO*	0.15	0.00	8.10	10.08	0.12	0.04	0.02	10.35	1.64	0.09	0.07	7.41**
MnO	0.00	0.00	0.13	0.06	0.01	0.00	0.00	0.31	0.00	0.00	0.01	0.02
MgO	0.06	0.00	12.93	17.56	0.04	0.00	0.00	11.33	2.55	0.07	0.01	0.05
ZnO									0.09	0.00	0.00	0.00
BaO									0.00			
CaO	19.07	9.62	23.91	12.64	20.72	19.47	15.62	24.70	0.07	19.52	12.37	23.80
Na_2O	2.80	8.09	0.31	0.20	1.75	0.45	2.74	0.12	0.18	2.34	6.49	0.00
K_2O	0.24	0.73	0.00	0.07	0.15	0.02	0.08	0.02	10.90	0.41	0.58	0.00
F	0.06	0.00		0.00	0.03				0.07	0.00	0.00	0.00
Cl	0.22	2.63		0.00	0.07				0.00	0.36	1.61	0.00
O=F, Cl	0.07	0.59		0.00	0.03				0.03	0.08	0.36	0.00
Total	95.73	98.93	100.03	97.58	95.20	99.76	100.56	100.76	95.40	95.24	97.92	90.44
Formula												
O	16†	16†	6	23	16†	8	8	6	11	16†	16†	12.5
Si	6.92	7.97	1.96	7.75	6.67	2.05	2.25	1.98	3.13	6.81	7.62	3.02
Ti	0.00	0.00	0.00	0.02	0.00	0.00	0.00	0.00	0.00	0.00	0.00	0.00
Al	5.05	4.10	0.08	0.35	5.31	1.94	1.74	0.04	2.61	5.16	4.44	2.55
Cr	0.00	0.00	0.00	0.01	0.00	0.00	0.00	0.00	0.00	0.00	0.00	0.00
Fe^{3+}				0.13§								0.43**
Fe^{2+}*	0.02	0.00	0.25	1.07§	0.02	0.00	0.00	0.33	0.09	0.01	0.01	
Mn	0.00	0.00	0.00	0.01	0.00	0.00	0.00	0.01	0.00	0.00	0.00	0.00
Mg	0.01	0.00	0.72	3.71	0.01	0.00	0.00	0.64	0.25	0.02	0.00	0.01
Zn									0.00	0.00	0.00	0.00
Ba									0.00			
Ca	3.13	1.50	0.96	1.92	3.43	0.97	0.76	0.99	0.01	3.23	1.96	1.99
Na	0.83	2.29	0.02	0.06	0.52	0.04	0.24	0.01	0.02	0.70	1.86	0.00
K	0.05	0.14	0.00	0.01	0.03	0.00	0.01	0.00	0.93	0.08	0.11	0.00
Total	16.00	16.00	4.00	13.83	16.00	5.00	5.00	4.00	7.04	16.00	16.00	7.56
F	0.03	0.00		0.00	0.02				0.02	0.00	0.00	0.00
Cl	0.06	0.65		0.00	0.02				0.00	0.09	0.40	0.00

* Total iron as FeO.

** Total iron as Fe_2O_3.

† Total cations as 16.

§ Calculated value (see text).

Abbreviations for texture: Pgp, prograde phase; Rgp, retrograde phase.

Table 4. Chemical compositions of minerals employed for the calculations of T-X_{CO2} diagrams.

Sample	Chu	Tr		Di	Scp		Pl		Czo	Figure
	X_F	X_{OH}	X_{Mg}	X_{Mg}	*EqAn*		*An*		X_{Fe}	
	Pgp	Pgp	Rgp	Pgp	Pgp	Rgp	Pgp	Rgp	Rgp	
KST03	0.63	0.80		1.00						Fig. 11
OZ03					68		82*			Fig, 12
WBY01					78		95			Fig, 12
KB01			0.80**	0.80	70		85*		0.15	Fig. 13a
KB01						65		78*	0.15	Fig. 13b

* Anorthite content was estimated assuming that $An/EqAn = 1.2$ considering the pair of prograde scapolite and plagioclase in WBY01.

** X_{Mg} value was assumed to be same with that of diopside.

Abbreviations for texture: Pgp, prograde phase; Rgp, retrograde phase.